Modeling and Application of a Thermoelectric Generator

by

David Yan

A thesis submitted in conformity with the requirements
for the degree of Masters of Applied Science
Graduate Department of Electrical and Computer Engineering
University of Toronto

Abstract

Modeling and Application of a Thermoelectric Generator

David Yan

Masters of Applied Science

Graduate Department of Electrical and Computer Engineering

University of Toronto

2011

Thermoelectric modules are an important alternative to heat engines in the harvesting of waste heat. Electrical-thermal analogues are often employed when studying heat conduction and this analogue can be extended to develop an equivalent circuit for thermoelectric effects. For the primarily one-dimensional problem of thermoelectricity, the equations can be discretized to create a simple mathematical model. In this document, such a model is developed from first principles and show that the electro-thermal coupling is properly incorporated. The results of simulations using the model are then presented and validated experimentally. Furthermore, in one possible application of thermoelectric modules, a self-contained cooling unit with an integrated thermoelectric generator is designed. By performing fluid dynamics simulations on a fan and heat sink model, the geometry and operating conditions can be optimized and the start-up and transient characteristics are studied.

Contents

List of Figures

Chapter 1

Introduction

1.1 Background

Waste heat is heat produced as a byproduct in power generation, industrial processes and electrical machines, among others. Vast amounts of waste heat are produced by industry. In addition, low-grade heat (heat sources roughly under 100 C)[1] is also available from natural sources such as geothermal reservoirs and solar energy. Recovering this heat into usable electricity would save a significant amount of money through increasing efficiency and lowering fuel costs as well as being beneficial to the environment.[2] For any heat engine, the laws of thermodynamics place fundamental constraints on the amount of useful power which can be extracted. Owing to the need for any generation process to discard heat, the fraction of heat which may be converted depends on the intake and exhaust temperature, with lower temperatures being less efficient. However, since such a large amount of energy is freely available, the engineering problem then becomes one of economics, and choosing the technology and configuration which produces the best utilization of heat.

In the case of heat recovery, the technologies to do so already exist and are already in use. The two most prominent technologies used in this application are those derived from

heat engines and those derived from thermoelectricity. The Rankine cycle, often used in power plants, is a heat engine which uses the phase change of steam or another working fluid to drive a turbine and generate electricity. At low temperatures, organic working fluids with low boiling points are used instead of steam to increase efficiency, and this process is termed the Organic Rankine Cycle (ORC). Thermoelectric generators, which are semiconductor junction type devices, use the thermoelectric effect to convert heat to electricity and vice versa. They have the advantage of being very simple with no moving parts, requiring low maintenance and are therefore able to be used for sources of heat for which the organic Rankine cycle would be inapplicable, such as those located in remote or hostile environments.[1] For example, in space applications, consideration is given to their low weight and reliability compared to heat engines. [3]

1.2 Physics of Thermoelectric Materials

Due to the phenomena of electron and phonon transport in conductors and semiconductors, electrical current and heat flux are, in general, coupled and linear functions of the electric field and the gradient of temperature [4][5], i.e.:

$$\mathbf{J} = \sigma\mathbf{E} - \sigma\alpha\nabla T \quad \left(\frac{A}{m^2}\right) \tag{1.1}$$

$$\mathbf{q} = \pi\mathbf{J} - k\nabla T \quad \left(\frac{W}{m^2}\right) \tag{1.2}$$

Where $\mathbf{E}$ and T are the electric field and temperature, respectively, α is the Seebeck Coefficient, π is the Peltier Coefficient, σ is the electrical conductivity and k is the thermal conductivity. However,even without knowing exactly what the coefficients (α, π, σ, k) are, it is clear from equations (1.1) and (1.2) that in any material which allows both electrical and heat conduction,

1. a temperature gradient causes an electric field to develop in the absence of electrical current, and

2. an electric field causes a thermal gradient to develop in the absence of thermal current.

For a derivation of the transport equations, refer to Appendix A.

In 1821 Thomas Johann Seebeck discovered that a circuit composed of two different metals could deflect a compass needle when a temperature gradient was applied across it. This is termed the Seebeck effect, and its associated Seebeck coefficient α, is defined as:

$$\alpha\left(T\right) = \frac{\mathbf{E}}{\nabla T} \approx \frac{\Delta V}{\Delta T} \quad \left(\frac{V}{K}\right) \tag{1.3}$$

Jean-Charles Peltier discovered what is known as the Peltier effect in 1834, namely that current passing through the junction of two dissimilar materials caused heating or cooling at the junction. The Peltier coefficient π is the ratio of the rate of heat flux q to current density in the absence of a temperature gradient:

$$\pi(T) = \frac{\mathbf{q}}{\mathbf{J}} = \frac{Q}{I} \tag{1.4}$$

with units of Watts per Ampere.

The Peltier and Seebeck effects are also not independent, as was predicted by Lord Kelvin and experimentally shown. α and π are related through the second Kelvin relation:

$$\alpha(T) = \frac{\pi\left(T\right)}{T} \tag{1.5}$$

which shows that the Seebeck coefficient alone is enough to provide all of the thermoelectric properties of a material. A brief discussion of this relationship can be found in Appendix B.

The more familiar quantities of electrical conductivity (σ) and thermal conductivity (k) are defined as:

$$\sigma\left(T\right) = \frac{\mathbf{J}}{\mathbf{E}} \quad \left(\frac{S}{m}\right) \tag{1.6}$$

and

$$k\left(T\right) = -\frac{\mathbf{q}}{\nabla T} \quad \left(\frac{W}{mK}\right) \tag{1.7}$$

Equations (1.1) and (1.2) are the theoretical basis of the thermoelectric effect. However, note that although both the Seebeck and Peltier effects may appear to require the junction of two dissimilar materials, neither is a contact effect and both arise due to the presence of temperature gradients in the bulk.

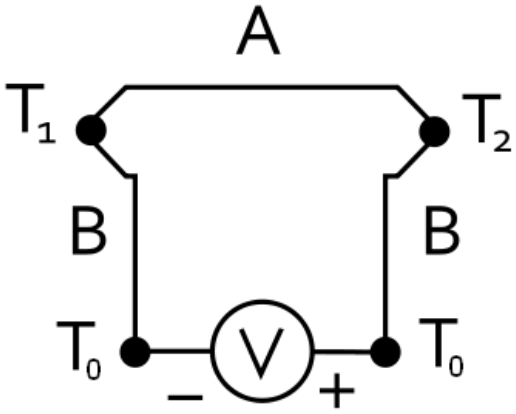

Figure 1.1: Thermoelectric Circuit

Experimentally, it is difficult to measure the absolute Seebeck coefficient of a single material since the same temperature difference that is applied across the material under test will also be applied across the measurement apparatus. For instance, in Figure 1.1, if material A is the material under test, material B is the material of the voltmeter leads and a temperature difference of T_1 - T_2 is put across material A, then the voltmeter is at some intermediate temperature T_0 and the voltage measured is:

$$V = -\int E \cdot dl = -\int \alpha \frac{dT}{dl}\, dl = \int_{T_0}^{T_1} \alpha_B \, dT + \int_{T_1}^{T_2} \alpha_A \, dT + \int_{T_2}^{T_0} \alpha_B \, dT \qquad (1.8)$$
$$= \int_{T_1}^{T_2} \alpha_A \, dT + \int_{T_2}^{T_1} \alpha_B \, dT = \int_{T_1}^{T_2} \alpha_A - \alpha_B \, dT$$

showing that it is only possible to measure the *difference* in Seebeck coefficients of two materials. However, it is still useful from a practical perspective to define absolute Seebeck coefficients, since most common conductive materials have negligible Seebeck coefficients and in practice the situation presented in figure 1.1 will constitute a measurement of α_A.

Also, due to the properties of semiconductors, n-type and p-type materials have Seebeck coefficients of opposing signs. (See the expressions (A.18) and (A.34) for α in Appendix A) For this reason, thermoelectric modules almost always consist of two semiconductor materials which appear electrically in series and thermally in parallel, as shown in figure 1.2.

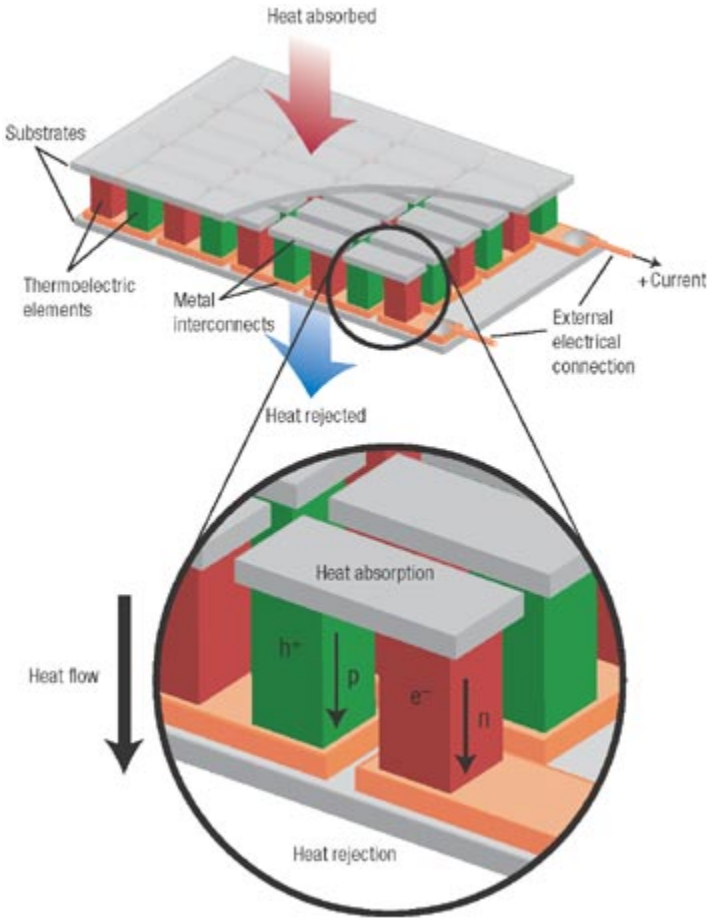

Figure 1.2: Thermoelectric Module

1.2.1 Efficiency

The efficiency of the type of thermoelectric module shown in figure 1.3 can be written as:

$$\eta_{max} = \frac{T_H - T_L}{T_H} \frac{\sqrt{1 + \frac{Z(T_H+T_L)}{2}} - 1}{\sqrt{1 + \frac{Z(T_H+T_L)}{2}} + \frac{T_L}{T_H}} \tag{1.9}$$

(1.9) is in the form of the ideal Carnot efficiency multiplied by a factor, which is a function of the so-called "figure of merit" Z, defined as:

$$Z = \frac{\alpha^2 \sigma}{k} \tag{1.10}$$

where α is the Seebeck coefficient, σ is the electrical conductivity and k is the thermal conductivity. In some literature, an alterative figure of merit, ZT, which actually denotes $\frac{Z(T_L+T_H)}{2}$, is employed instead. Research into materials for thermoelectric properties primarily focuses on improving this figure of merit. Refer to Appendix C for further discussion of the efficiency and figure of merit.

When choosing the material to use for a thermoelectric generator, it is most worthwhile to look at the three values which make up the figure of merit Z. The electrical conductivity σ is a measure of charge carrier concentration, of which metals have the highest while insulators have very low concentration and semiconductors lie somewhere in the intermediate. Thermal conductivity also increases with increasing carrier concentration. The Seebeck coefficient, on the other hand, decreases with increasing carrier concentration [2]. Semiconductors generally have the highest figures of merit due to having the best combinations of the three properties and nearly all modern thermoelectric materials are semiconductors.

Modern commercial thermoelectric semiconductor materials can be divided into three temperature ranges: Low temperature ($<$ 450 K) alloys use bismuth in combination with antimony, tellurium and selenium, medium range (850 K) materials are based on lead telluride and high temperature (up to 1300 K) materials are based on silicon and germanium [2].

Most commercially available thermoelectric devices consist of a large number of thermocouples connected in series and sandwiched between a thermally conductive hot plate and cold plate. Since the voltage output of a single semiconductor thermocouple is low (on the order of hundreds of microvolts per degree), many elements need to be in series in order to reach a reasonable voltage and be compatible with the operating voltages of

most transistors. Each thermocouple module then consists of a p-type leg and an n-type leg, since α is positive for p-type semiconductors and negative for n-type semiconductors. In order to maximize efficiency, some modern modules are also segmented or cascaded, which is to say that a single leg may use multiple materials in series. This is due to the fact that thermoelectric modules often see temperature gradients of hundreds of degrees, and since the figure of merit for a single material may change significantly over the temperature range, it becomes advantageous to use more than one material [2]. Also, the metal-semiconductor junctions in a thermoelectric module are ohmic contacts, meaning that the device is essentially symmetrical and can pump heat or current in either direction. Figure 1.3 shows a diagram of a segmented thermoelectric module with ohmic junctions.

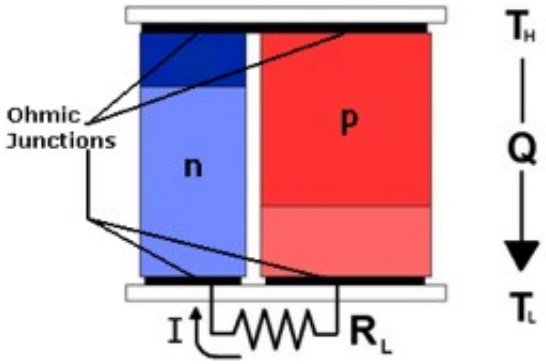

Figure 1.3: Segmented Generator

1.2.2 VI Characteristic

Figure 1.4 shows a measured VI characteristic and its corresponding power curve for a commercial TE module with 20 Watts of heat flux applied to the high side. A peak can be seen in the power curve and thus there is one electrical operating point for each set of temperature boundary conditions for which the output power is maximized. This is similar to the power curve for photovoltaic cells.

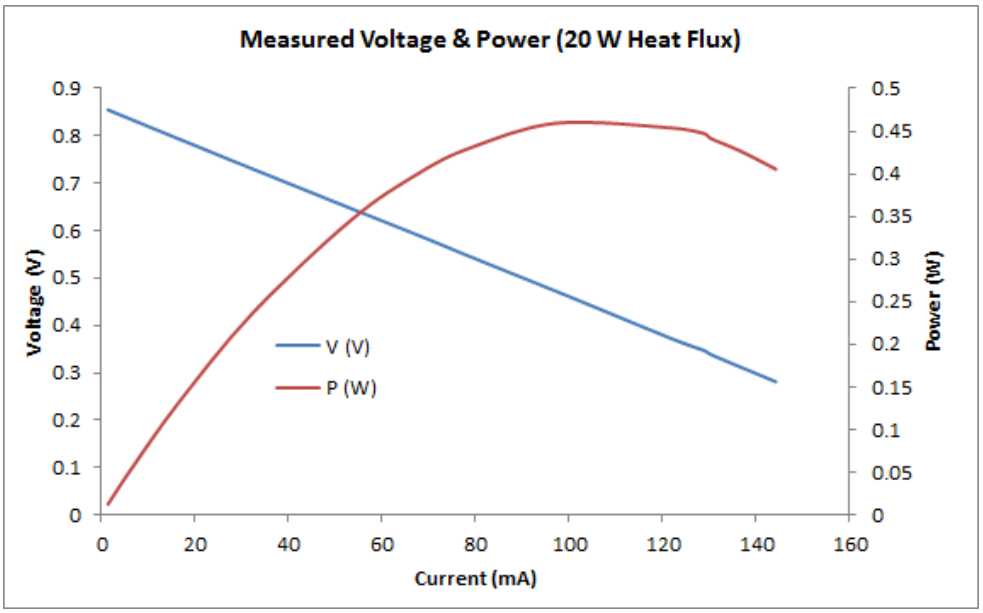

Figure 1.4: Measured VI and Power Curves

Though thermoelectricity is a nonlinear effect in temperature and voltage, the nonlinearity is small at low temperature differences and currents, and the rough location (treating the Seebeck voltage as an ideal source) of the peak power in terms of current is given in equation 1.11.

$$I_{P_{max}} \approx \frac{\alpha\,(T_H - T_L)}{2R_{te}} \tag{1.11}$$

where R_{te} is the electrical resistance of the thermoelectric module.

1.3 The Organic Rankine Cycle

An alternative to thermoelectricity for power generation is the heat engine. The thermodynamic process used most commonly for power generation is the Rankine Cycle. Here we briefly outline the steps in the cycle and its efficiency.

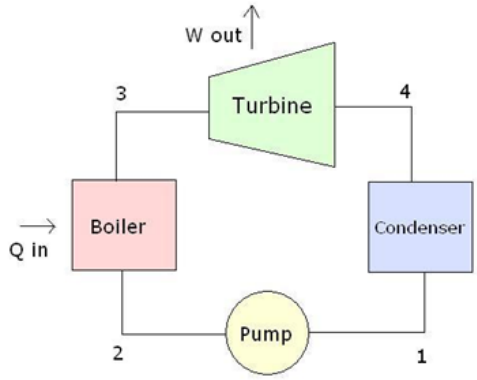

Figure 1.5: Rankine Cycle

The ideal Rankine cycle has the following legs as described below with reference to figure 1.5:

- 1-2 (Pump): Isentropic compression. Working fluid is pumped from the low pressure condenser to the high pressure evaporator
- 2-3 (Boiler): Isobaric heat input. Working fluid is evaporated into a dry vapor and fed into the turbine
- 3-4 (Turbine): Isentropic expansion. Vapor expands through a turbine, generating power
- 4-1 (Condenser): Isobaric heat rejection. Vapor is condensed back into a fluid and then recycled back into the boiler

1.3.1 Efficiency

The efficiency of the cycle depends on the choice of the working fluid. Water (steam) is generally used for power generation purposes, but at lower temperatures water is no longer thermodynamically favorable as a working fluid due to its saturated vapour curve. Therefore, in order to recover power from low grade waste heat, organic fluids which have

lower boiling points than water are used instead, and this is termed the Organic Rankine Cycle (ORC). The efficiency, η, is given by:

$$\begin{aligned} \eta &= \frac{(H_3 - H_4) - (-\Delta W_p)}{H_3 - H_2} \\ &\approx \frac{C_p\,(T_3 - T_4)}{C_p\,(T_3 - T_4) + \lambda_R - (-\Delta W_{pump})} \end{aligned} \tag{1.12}$$

where $H_3 - H_4$ is the energy generated in leg 3-4, $H_3 - H_2$ is the energy input in leg 2-3 and $(-\Delta W_p)$ represents parasitic losses. C_p is the heat capacity of the vapor, λ_R is the latent heat of vaporization and $(-\Delta W_{pump}) = H_2 - H_1$ denotes the energy required for the pumping phase. The full derivation for this expression can be found in Appendix C

Current applications of the ORC include waste heat recovery from industrial processes as well as solar and geothermal power generation. The literature describes an ORC intended to cool technical equipment such as a transformer, with electrical generation as a byproduct. In such a configuration, the device would receive cooling from an intermediate fluid which would then act as the heat reservoir for the "boiler" component of the ORC [6].

1.4 Objectives

The primary objective of this project is to develop a new and more accurate model of a thermoelectric generator by applying the finite volume method to the phenomenological equations of thermoelectricity. Using the discretized equations, a simple equivalent circuit can be created to aid in visualization. A secondary aim will be to design a self-contained cooling unit with an integrated thermoelectric generator. Specifically, it will be seen whether a thermoelectric generator integrated into a heat sink and fan can provide enough power to run the cooling fan in closed loop. By performing fluid dynamics simulations on the fan and heat sink model, it can be determined for what geometry and under what operating conditions a thermoelectric generator can power a cooling fan.

1.5 Thesis Outline

The chapters and appendices are organized as follows:

In chapter 2, existing one-dimensional models of thermoelectric devices are discussed and a new model based on the finite volume method (FVM) is developed, resulting in a coupled system of time-dependent partial differential equations. A discretization process is applied to the system, with careful attention paid to flux balance at the internal boundaries. The resulting system of coupled ordinary differential equations is simulated using Matlab and compared to experimental results.

In chapter 3, one possible application of thermoelectric generators is explored. An integrated heat sink-thermoelectric generator assembly is designed and tested for its electrical and thermal properties. Finite element (FEM) simulations in COMSOL are performed on the design in order to optimize the geometry. It was found that using the optimal geometry, there is a range of operating points under which it is possible for a thermoelectric module to power a cooling fan.

Appendix A presents a derivation of the transport equations (1.1) and (1.2) from the Boltzmann equation, which is a transport equation from statistical mechanics. In the derivation, a relaxation time approximation is used to show that the form of (1.1) and (1.2) is correct while avoiding the use of quantum mechanics to calculate transition rates. The validity of this approximation is also discussed.

Appendix B is a brief discussion of the Kelvin relation (equation (1.5)), presenting a line of reasoning based on thermodynamics.

Appendix C gives the full derivation for the efficiency and figure of merit for thermoelectric modules (equations (1.9) and (1.10), respectively), as well as the derivation for the efficiency for the Rankine Cycle (equation (1.12)).

Appendix D presents the mathematics behind a commercial FEM software package (COMSOL) model of a thermocouple. The model accounts for the temperature dependence of the transport coefficients. The COMSOL model was used to verify the results

from both the experiment and the finite volume simulation in Chapter 2.

Appendix E gives the details of the experimental apparatus which was constructed to verify the simulation results.

Appendix F contains the MATLAB code used to simulate the model developed in Chapter 2.

Chapter 2

Finite Volume Model of Thermoelectric Module

2.1 Introduction

Thermoelectric modules are energy conversion devices which can either convert heat to electricity or operate in reverse as a heat pump. Despite relatively low efficiency, their solid-state nature allows them to be used in applications such as harvesting waste heat where a heat engine would be impractical.

The physics of thermoelectricity can be modeled at several levels: quantum mechanical, statistical mechanical and at a macroscopic level using the transport equations directly. Though using quantum mechanics is the only way to most accurate way to approximate the basic material properties, from the Boltzmann equation (statistical mechanics) one can derive the phenomenological transport equations (see Appendix A). The phenomenological equations are far more practical and just as accurate provided the necessary material properties are known from experiment.

Equivalent circuit models are often used to model heat conduction, and the basis of both electrical and thermal circuits is a mathematical discretization of their respective

diffusion equations. By applying the same discretization process, it is possible to solve the coupled thermoelectric equations with a great deal of accuracy. Once the discretized equations are obtained, an equivalent circuit can be easily built as a visualization tool. However, creating such a model is not straightforward due to the coupled and nonlinear nature of the transport equations, and difficulties in treating flux balance at the boundaries.

Solving the physics of thermoelectricity is a three-dimensional problem which is one-dimensional to first approximation due to a combination of factors: (1) the geometry of the material, (2) the regime that commercial thermoelectric modules are being operated in and (3) the scale of the effects we are interested in. The 1-D problem can be modeled using a variety of numerical approaches. The same numerical methods are equally valid for the equivalent three-dimensional problem, but the one-dimensional model is easier to code up, faster to compute, and easier to visualize using a circuit model. The finite volume method is the chosen discretization used in this work because conceptually it is the one that most easily deals with the flux equations found in systems of electrical and thermal transport. It is worth noting, however, that in problems with only one dimension there is not much difference between the various flavours of discretization, and all are in fact just applying the fundamental theorem of calculus to a function on a domain. This chapter presents present the discretized system and the results from the simulations.

2.2 Review of Thermoelectric Models

Many one-dimensional models exist for thermoelectric materials. The majority of these fall under the category of circuit-based models or analytical models, both of which tend to omit some of the physics in order to get a simpler picture. This section presents an overview of some popular models.

Circuit models are attractive due to their simplicity and the convenience of obtaining

quick results from circuit simulators. These models range from relatively simple lumped equivalent circuits[7] [8] [9] to distributed circuits [10][11]. The basis of these models is the idea of expanding on an electro-thermal analogue circuit[12] by adding nonlinear current sources to account for the thermoelectric effect. This method, while valuable for simplicity and visualization, requires one to make many unstated assumptions. These assumptions are usually extreme simplifications meant for quick calculations of important values.

Furthermore, commercial circuit simulators are, in general, inadequate in dealing with distributed circuits of the complexity required to satisfactorily model a thermoelectric device. This is mainly due to the difficulty of manipulating a nonlinear distributed circuit. For instance, many programs are unable to create nonlinear dependent sources (of voltage and temperature) or distributed circuits containing non-fixed circuit elements. This results in the scope of some models being limited by the capabilities of commercial software packages.

An analytical model which appears frequently in textbooks [13][14] on the subject treats the thermoelectric material as one block with transport coefficients which are constant throughout the material, and is used to establish an expression for the figure of merit. The two ubiquitous equations used for this simple model are:

$$Q_H = K\left(T_H - T_L\right) + \left(\alpha_p - \alpha_n\right) T_H I - \frac{1}{2} I^2 R \tag{2.1}$$

$$\Delta V = \left(\alpha_p - \alpha_n\right)\left(T_H - T_L\right) \tag{2.2}$$

which states that the high side heat power is the sum of the conduction, Peltier and Joule ($\frac{1}{2}I^2R$, where R is the electrical resistance of the thermoelectric module) terms and the voltage is the combined Seebeck coefficient of the p-type and n-type legs times the temperature difference. Using these equations (and the equivalent equation for heat at the low side), it is indeed possible to calculate an approximate value for the voltage difference or heat flux. However, there are obviously flaws with such a simple model. For

example, the $\frac{1}{2}I^2R$ term in equation (2.1) arises from the oft-stated but rarely justified claim that exactly half of the Joule heat flows to each end of the device.

Overall, some shortcomings of existing models may be identified as follows:

- Not allowing for transport coefficients that depend on temperature. Indeed, experiments show that the three transport coefficients (the Seebeck coefficient, electrical conductivity and thermal conductivity) are significantly temperature dependent in the low to medium temperature range. The Seebeck coefficient especially can vary significantly even in a relatively small temperature range[15][16], and therefore all three coefficients, and the Seebeck coefficient in particular, should be modeled as functions of temperature. Very rarely in the literature are models with temperature-dependent coefficients proposed (but see [11]).

- Not including a model of the high side and low side heat sinks/heat exchangers. In any real physical application of a thermoelectric device, there must be a heat source and sink to transport the heat flux to and from the device. When modeling the dynamics of the system, these will almost always have a much larger heat capacity than the thermoelectric device itself, and will therefore play a large role in the transient response. Some models [7] do include the high side and low side thermal circuits, but these components are not modeled using distributed circuits or given as much attention as the thermoelectric model.

- Most important of all is the mathematical implementation of the flux balance at the interface between the thermoelectric material and the heat sinks, which to the author's knowledge has not been examined in the literature.

We propose to discretize the modeling PDEs directly, thus bypassing the need for a circuit model. This way, all assumptions are known and the model can be easily related back to the original physics. Furthermore, in the discretization process one can adjust the accuracy and level of complexity of the model by choosing alternate approximations

for the boundary conditions, the transport coefficients, and the like. While an equivalent circuit representation for the discretized system may be possible, it would only be of secondary importance.

2.3 The Modeling Equations and Boundary Conditions

The system consists of three domains with four boundaries. The subdomains and their equations are shown in figure 2.1.

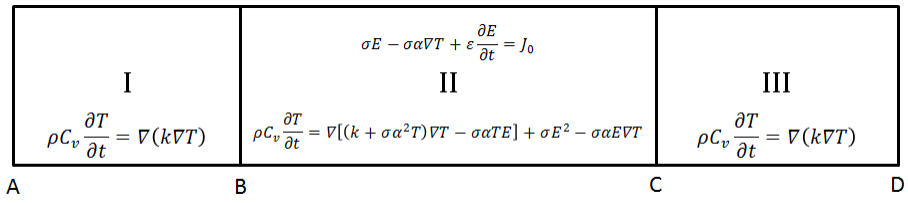

Figure 2.1: Subdomain Equations

Subdomains I and III represent the heat source and sink, respectively, and subdomain II represents the thermoelectric material. The time-dependent thermoelectric equations shown in figure 2.1 can be obtained by substituting equations (1.1) and (1.2) into the charge and heat flux conservation equations (equations (2.3) and (2.4)), shown below.

$$\nabla \cdot \mathbf{J} + \frac{\partial \rho}{\partial t} = 0 \tag{2.3}$$

$$\nabla \cdot \mathbf{q} + \rho C_v \frac{\partial T}{\partial t} = \dot{Q} = \mathbf{E} \cdot \mathbf{J} \tag{2.4}$$

The thermal boundary conditions are:

- A: A heat flux q_0 is imposed ($-k\frac{\partial T}{\partial x} = q_0$)

- B: The heat is continuous across the interface (flux balance); A current J_0 is imposed ($J = J_0$)
- C: The heat is continuous across the interface (flux balance);, A voltage V_0 is imposed ($V = 0$)
- D: A temperature T_{amb} is imposed ($T = T_{amb}$)

It is assumed that k, ρC_v, ϵ and σ are constant within each subdomain; they can (and will) differ between domains due to material differences. In subdomain II, $\alpha = \alpha(T)$ is a function of temperature, as the voltage gradient created by the Seebeck coefficient is the quantity we are most interested in. Assuming that k, ρC_v, etc are constant simplifies the development of the equations somewhat. That said, should the model be needed in a regime where these quantities depend on either temperature or electric field then the methods presented for $\alpha(T)$ would generalize directly.

2.4 The Finite Volume Method

In the finite volume method, each domain is divided into intervals (or meshes), each one of length Δx, centered about x_i with endpoints $x_{i-1/2}$ and $x_{i+1/2}$. Functions of x such as temperature $T(x,t)$ are then averaged over the ith interval to become $\overline{T}_i(t)$ using a differencing scheme, such as the one in equation (2.5). Similarly, $T_x(x,t)$ is approximated by $T_x(x_i,t)$ as in equation (2.6), and so forth. As long as the intervals have the same length, Δx, this approximation is second-order accurate for functions that have bounded second derivatives in space. The discretization scheme used on the bulk in this work is shown for T below:

$$\overline{T}_i(t) := \frac{1}{\Delta x}\int_{x_{i-1/2}}^{x_{i+1/2}} T(x,t)\, dx \tag{2.5}$$

$$\frac{1}{\Delta x}\int_{x_{i-1/2}}^{x_{i+1/2}} \frac{\partial T}{\partial x}(x,t)\, dx \approx \frac{T\left(x_{i+1/2},t\right) - T\left(x_{i-1/2},t\right)}{\Delta x} \approx \frac{\overline{T}_{i+1}(t) - \overline{T}_{i-1}(t)}{2\Delta x} \tag{2.6}$$

$$\frac{1}{\Delta x}\int_{x_{i-1/2}}^{x_{i+1/2}} \frac{\partial^2 T}{\partial x^2}(x,t)\,dx \approx \frac{\frac{\partial T}{\partial x}\left(x_{i+1/2},t\right)-\frac{\partial T}{\partial x}\left(x_{i-1/2},t\right)}{\Delta x} \approx \frac{\frac{\overline{T}_{i+1}(t)-\overline{T}_i(t)}{\Delta x}-\frac{\overline{T}_i(t)-\overline{T}_{i-1}(t)}{\Delta x}}{\Delta x} = \frac{\overline{T}_{i+1}(t)-2\overline{T}_i(t)+\overline{T}_{i-1}(t)}{(\Delta x)^2} \tag{2.7}$$

and E is handled in the same fashion.

Another approximation which must be made frequently is that the average of a product is approximately equal to the product of the averages. It can be shown that $\overline{\Pi U} = \Pi\overline{U} + \mathcal{O}(\Delta x^2)$, or that the error is second order in Δx.

2.5 Heat equation on subdomains I and III

This section contains the discretization of the heat equation (equation (2.8)) on the bulk of subdomains I and III. Note that while we use k and Δx here for the derivation for simplicity, they are in general different between the two subdomains.

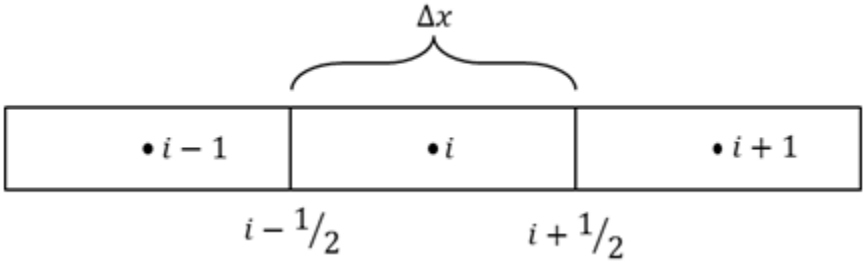

Figure 2.2: Mesh Nodes in Subdomain I and III Bulk

$$\rho C_v \frac{\partial T}{\partial t} = \frac{\partial}{\partial x}\left(k\frac{\partial T}{\partial x}\right) \tag{2.8}$$

$$\frac{1}{\Delta x}\int_{i-1/2}^{i+1/2} \rho C_v \frac{\partial T}{\partial t}\,dx = \frac{1}{\Delta x}\int_{i-1/2}^{i+1/2} \frac{\partial}{\partial x}\left(k\frac{\partial T}{\partial x}\right)\,dx \tag{2.9}$$

$$\rho C_v \frac{\partial \overline{T_i}}{\partial t} = \frac{k}{\Delta x}\left[\left(\frac{\partial T}{\partial x}\right)_{i+1/2} - \left(\frac{\partial T}{\partial x}\right)_{i-1/2}\right] \tag{2.10}$$

$$\rho C_v \frac{\partial \overline{T_i}}{\partial t} = \frac{k}{\Delta x}\left[\left(\frac{\overline{T_{i+1}} - \overline{T_i}}{\Delta x}\right) - \left(\frac{\overline{T_i} - \overline{T_{i-1}}}{\Delta x}\right)\right] \tag{2.11}$$

2.6 TE Equations in subdomain II

This section contains the discretization of the thermoelectric equations (equations (2.12) and (2.13)) on the bulk (subdomain II).

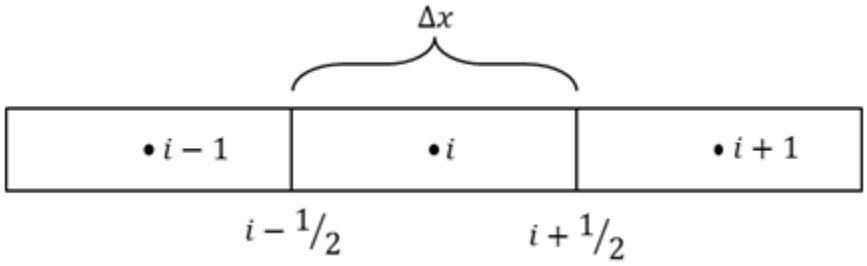

Figure 2.3: Mesh Nodes in Subdomain II Bulk

$$\rho C_v \frac{\partial T}{\partial t} = \sigma E^2 - \sigma\alpha E\frac{\partial T}{\partial x} + \frac{\partial}{\partial x}\left[\left(k + \sigma\alpha^2 T\right)\frac{\partial T}{\partial x} - \sigma\alpha T E\right] \tag{2.12}$$

$$\epsilon\frac{\partial E}{\partial t} = J_0 - \sigma E + \sigma\alpha\frac{\partial T}{\partial x} \tag{2.13}$$

$$\frac{1}{\Delta x}\int_{i-1/2}^{i+1/2} \rho C_v \frac{\partial T}{\partial t}\,dx = \frac{1}{\Delta x}\int_{i-1/2}^{i+1/2} \sigma E^2 - \sigma\alpha E\frac{\partial T}{\partial x} + \frac{\partial}{\partial x}\left[\left(k + \sigma\alpha^2 T\right)\frac{\partial T}{\partial x} - \sigma\alpha T E\right] dx \tag{2.14}$$

$$\frac{1}{\Delta x}\int_{i-1/2}^{i+1/2} \epsilon\frac{\partial E}{\partial t}\,dx = \frac{1}{\Delta x}\int_{i-1/2}^{i+1/2} J_0 - \sigma E + \sigma\alpha\frac{\partial T}{\partial x}\,dx \tag{2.15}$$

$$\rho C_v \frac{\partial \overline{T_i}}{\partial t} = \sigma\overline{E_i}^2 - \sigma\overline{\alpha_i}\overline{E_i}\frac{T_{i+1/2} - T_{i-1/2}}{\Delta x} + \frac{k}{\Delta x}\left[\left(\frac{\partial T}{\partial x}\right)_{i+1/2} - \left(\frac{\partial T}{\partial x}\right)_{i-1/2}\right] \tag{2.16}$$
$$+\frac{\sigma\overline{\alpha_i}^2}{\Delta x}\left[\left(T\frac{\partial T}{\partial x}\right)_{i+1/2} - \left(T\frac{\partial T}{\partial x}\right)_{i-1/2}\right] - \frac{\sigma\overline{\alpha_i}}{\Delta x}\left[(TE)_{i+1/2} - (TE)_{i-1/2}\right]$$

$$\epsilon\frac{\partial \overline{E_i}}{\partial t} = J_0 - \sigma\overline{E_i} + \sigma\overline{\alpha_i}\frac{T_{i+1/2} - T_{i-1/2}}{\Delta x} \tag{2.17}$$

$$\rho C_v \frac{\partial \overline{T_i}}{\partial t} = \sigma \overline{E_i}^2 - \sigma \overline{\alpha_i} \overline{E_i} \frac{\overline{T_{i+1}} - \overline{T_{i-1}}}{2\Delta x} + \frac{k}{\Delta x}\left[\frac{\overline{T_{i+1}} - 2\overline{T_i} + \overline{T_{i-1}}}{\Delta x}\right] \tag{2.18}$$
$$+\frac{\sigma \overline{\alpha_i}^2}{\Delta x}\left[\frac{\overline{T_{i+1}} + \overline{T_i}}{2}\frac{\overline{T_{i+1}} - \overline{T_i}}{\Delta x} - \frac{\overline{T_i} + \overline{T_{i-1}}}{2}\frac{\overline{T_i} - \overline{T_{i-1}}}{\Delta x}\right]$$
$$-\frac{\sigma \overline{\alpha_i}}{\Delta x}\left[\frac{\overline{T_{i+1}} + \overline{T_i}}{2}\frac{\overline{E_{i+1}} + \overline{E_i}}{2} - \frac{\overline{T_i} + \overline{T_{i-1}}}{2}\frac{\overline{E_i} + \overline{E_{i-1}}}{2}\right]$$
$$\epsilon \frac{\partial \overline{E_i}}{\partial t} = J_0 - \sigma \overline{E_i} + \sigma \overline{\alpha_i} \frac{T_{i+1} - T_{i-1}}{2\Delta x} \tag{2.19}$$

Next, for the heat equations at the outside boundary we apply the boundary conditions to obtain the correct discretized equations.

2.7 Heat equation at boundary A

This section contains the discretization of the heat equation (equation (2.20)) at the leftmost boundary of the domain.

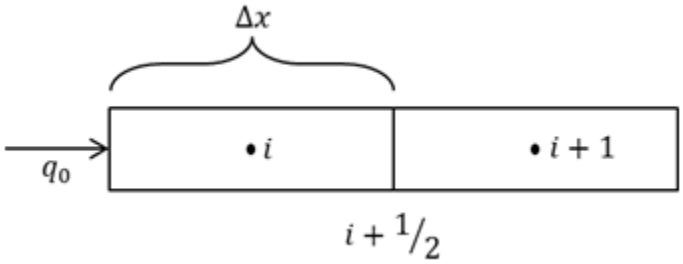

Figure 2.4: Boundary A

$$\rho C_v \frac{\partial T}{\partial t} = \frac{\partial}{\partial x}\left(k \frac{\partial T}{\partial x}\right) \tag{2.20}$$
$$\frac{1}{\Delta x}\int_{i-1/2}^{i+1/2} \rho C_v \frac{\partial T}{\partial t}\, dx = \frac{1}{\Delta x}\int_{i-1/2}^{i+1/2} \frac{\partial}{\partial x}\left(k \frac{\partial T}{\partial x}\right) dx \tag{2.21}$$
$$\rho C_v \frac{\partial \overline{T_i}}{\partial t} = \frac{k}{\Delta x}\left[\left(\frac{\partial T}{\partial x}\right)_{i+1/2} - \left(\frac{\partial T}{\partial x}\right)_{i-1/2}\right] \tag{2.22}$$

At this boundary, $-k\frac{\partial T}{\partial x} = q_0$, so:

$$\rho C_v \frac{\partial \overline{T_i}}{\partial t} = \frac{k}{\Delta x}\left[\left(\frac{\overline{T_{i+1}} - \overline{T_i}}{\Delta x}\right) - q_0\right] \tag{2.23}$$

2.8 Heat equation at boundary D

This section contains the discretization of the heat equation (equation (2.24)) at the rightmost boundary of the domain.

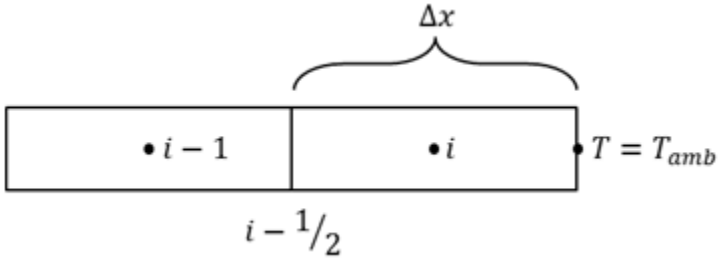

Figure 2.5: Boundary D

$$\rho C_v \frac{\partial T}{\partial t} = \frac{\partial}{\partial x}\left(k\frac{\partial T}{\partial x}\right) \tag{2.24}$$

$$\frac{1}{\Delta x}\int_{i-1/2}^{i+1/2} \rho C_v \frac{\partial T}{\partial t}\,dx = \frac{1}{\Delta x}\int_{i-1/2}^{i+1/2} \frac{\partial}{\partial x}\left(k\frac{\partial T}{\partial x}\right)\,dx \tag{2.25}$$

$$\rho C_v \frac{\partial \overline{T_i}}{\partial t} = \frac{k}{\Delta x}\left[\left(\frac{\partial T}{\partial x}\right)_{i+1/2} - \left(\frac{\partial T}{\partial x}\right)_{i-1/2}\right] \tag{2.26}$$

At this boundary, $T = T_{amb}$, so $\left(\frac{\partial T}{\partial x}\right)_{i+1/2}$ can be approximated as:

$$\left(\frac{\partial T}{\partial x}\right)_{i+1/2} \approx \frac{T_{amb} - \overline{T_i}}{\Delta x/2} \tag{2.27}$$

and thus the discretized equation is:

$$\rho C_v \frac{\partial \overline{T_i}}{\partial t} = \frac{k}{\Delta x}\left[\frac{T_{amb} - \overline{T_i}}{\Delta x/2} - \frac{\overline{T_i} - \overline{T_{i-1}}}{\Delta x}\right] \tag{2.28}$$

2.9 Heat and TE equations at boundaries B and C

In order to properly discretize the equations on the inner boundaries, we must first examine what is happening in the physical system. The paths for the electrical and thermal fluxes are shown in figure 2.6.

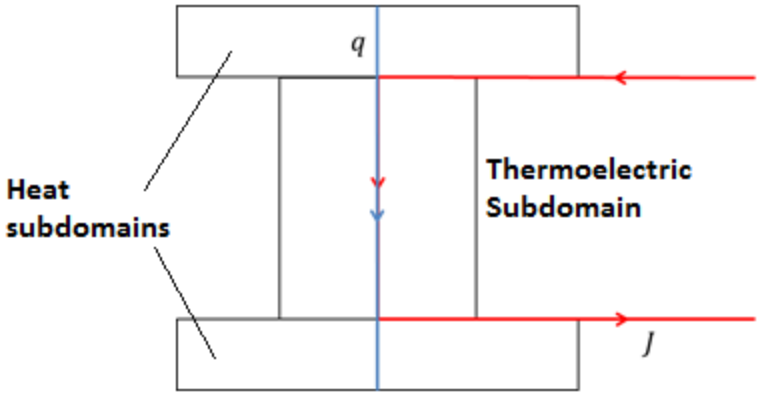

Figure 2.6: Paths for Electrical and Thermal Fluxes

The heat and electrical equations are only coupled in the thermoelectric material, subdomain II. In a real thermoelectric device, the electrical current would enter and leave via soldered wires while the heat flux flows through the top and bottom plates. Subdomains I and III represent the materials in the path of the heat flux and are included in the model because they contribute significantly to the transient response, while the electrical domains outside of the thermoelectric material are not modeled because they contribute very little. This presents a unique difficulty as, in the model, the boundaries are between a system of two coupled equations and a single equation on whose domain the electrical material properties are technically undefined. Moving forward, we must be more careful with our approximations and more precise with our definitions.

We will only derive the equations at boundary B, since an identical procedure can be used to find the equations at boundary C. It is also worth noting that there are two approaches to meshing at a material boundary: one mesh element straddling the boundary (mesh node on material boundary) or two mesh elements on either side of the boundary (mesh boundary on material boundary). In this analysis we choose not to straddle, since, when integrating, it is unclear how the electrical equations and coefficients should be defined in the half of the mesh residing in subdomains I and III.

Before tackling the issue of approximating the terms in the thermoelectric equations

at the boundary, let us examine the simpler case of the heat equation across a boundary where the thermal resistance changes.

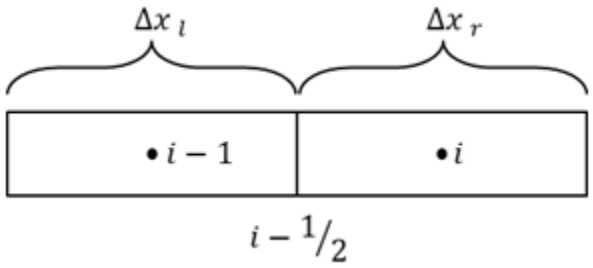

Figure 2.7: Heat Flux Across a Boundary

Let the cell on the left side be labeled $i-1$ and the cell on the right be labeled i, as shown in figure 2.7. By flux balance,

$$\lim_{x \to x_{i-1/2-}} \left(k \frac{\partial T}{\partial x} \right) = \lim_{x \to x_{i-1/2+}} \left(k \frac{\partial T}{\partial x} \right) \tag{2.29}$$

$$k_l \frac{T_{i-1/2} - T_{i-1}}{\Delta x_l / 2} = k_r \frac{T_i - T_{i-1/2}}{\Delta x_r / 2} \tag{2.30}$$

Solving for $T_{i-1/2}$, we have:

$$T_{i-1/2} = \frac{\frac{\Delta x_l}{k_l} \overline{T_i} + \frac{\Delta x_r}{k_r} \overline{T_{i-1}}}{\frac{\Delta x_l}{k_l} + \frac{\Delta x_r}{k_r}} \tag{2.31}$$

which indicates that this choice of $T_{i-1/2}$ satisfies flux balance. This approximation is well known to electrical engineers as it is the one made in circuit theory for resistor dividers. Plugging in this expression for $T_{i-1/2}$ back into the expression for the flux to the left of right of the boundary, we arrive at:

$$\left(k \frac{\partial T}{\partial x} \right)_l = \left(k \frac{\partial T}{\partial x} \right)_r = \frac{2 \left(\overline{T_i} - \overline{T_{i-1}} \right)}{\frac{\Delta x_l}{k_l} + \frac{\Delta x_r}{k_r}} \tag{2.32}$$

The next question is how to approximate $T_{i-1/2}$ with the thermoelectric domain on the right side of the boundary, since the way we approximate $T_{i-1/2}$ directly determines how we write $\frac{\partial T}{\partial x}_{i-1/2}$. The flux balance is now:

$$k_I \frac{\partial T}{\partial x} = \left(k_{II} + \sigma_{II} \alpha^2 T \right) - \sigma_{II} \alpha T E \tag{2.33}$$

This raises the question of how to approximate the electric field at the boundary B. Let us take a Gaussian surface at the boundary:

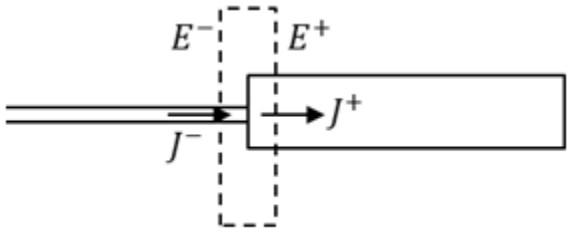

Figure 2.8: Gaussian Surface at boundary B

The left side, we have said, is a wire which we can approximate as having zero electric field and a forcing current density of J_0 and the right side is the thermoelectric material. The charge conservation equation and Gauss's law at the boundary shown in figure 2.8 is:

$$\nabla J + \frac{\partial \rho}{\partial t} = 0 \ , \ \nabla E = \frac{\rho}{\epsilon} \tag{2.34}$$

Taking the volume integral of over the volume enclosed by the surface of both equations, we have:

$$\int_V \nabla J \, dV + \frac{\partial}{\partial t} \int_V \rho \, dV = 0 \ , \ \int_V \nabla E \, dV = \frac{1}{\epsilon} \int_V \rho \, dV \tag{2.35}$$

$$\int_{\partial V} J \, dV + \frac{\partial}{\partial t} \int_V \rho \, dV = 0 \ , \ \int_{\partial V} E \, dV = \frac{1}{\epsilon} \int_V \rho \, dV \tag{2.36}$$

$$J^+ - J^- + \frac{\partial}{\partial t} \int_V \rho \, dV = 0 \ , \ E^+ - E^- = \frac{1}{\epsilon} \int_V \rho \, dV \tag{2.37}$$

We have assumed that E^-, the electric field in the conductor, is vanishing and the expressions for J^+ and J^- are known, so taking the derivative of the right equation and substituting it into the left one yields:

$$\epsilon \frac{\partial E^+}{\partial t} + \sigma_{II} E^+ - \sigma_{II} \alpha \nabla T - J_0 = 0 \tag{2.38}$$

This is actually just the same equation we have been using everywhere else on the thermoelectric domain. Thus, our system requires two additional differential equations

on boundaries B and C which is discretized as follows (at boundary B):

$$\epsilon\frac{\partial E_{i-1/2}}{\partial t} = J_0 - \sigma_{II}E_{i-1/2} + \sigma_{II}\alpha_i\frac{T_i - T_{i-1/2}}{\Delta x/2} = 0 \tag{2.39}$$

Now we can return to the heat flux balance at the boundary:

$$k_I\left(\frac{\partial T}{\partial x}\right)_l = k_{II}\left(\frac{\partial T}{\partial x}\right)_r + \sigma_{II}\alpha^2 T\left(\frac{\partial T}{\partial x}\right)_r - \sigma_{II}\alpha TE \tag{2.40}$$

Note that there are two ways to discretize the $\sigma_{II}\alpha^2 T\left(\frac{\partial T}{\partial x}\right)_r$ term in the above equation, either by substituting $T = T_{i-1/2}$, resulting in a quadratic equation for $T_{i-1/2}$, or by approximating $T = T_i$, resulting in a linear equation for $T_{i-1/2}$.

Depending on the choice for T at the boundary in equation (2.40), we can write:

$$\frac{T_{i-1/2} - \overline{T_{i-1}}}{\Delta x_I/2k_I} = \frac{\overline{T_i} - T_{i-1/2}}{\Delta x_{II}/2k_{II}} - \sigma_{II}\alpha^2\overline{T_i}\frac{\overline{T_i} - T_{i-1/2}}{\Delta x_{II}/2} - \sigma_{II}\alpha\overline{T_i}E_{i-1/2} \tag{2.41}$$

or:

$$\frac{T_{i-1/2} - \overline{T_{i-1}}}{\Delta x_I/2k_I} = \frac{\overline{T_i} - T_{i-1/2}}{\Delta x_{II}/2k_{II}} - \sigma_{II}\alpha^2\overline{T_{i-1/2}}\frac{\overline{T_i} - T_{i-1/2}}{\Delta x_{II}/2} - \sigma_{II}\alpha\overline{T_{i-1/2}}E_{i-1/2} \tag{2.42}$$

The linear solution for $T_{i-1/2}$ is:

$$T_{i-1/2} = \frac{\frac{\Delta x_{II}}{k_{II}}\overline{T_{i-1}} + \frac{\Delta x_I}{k_I}\overline{T_i} + \frac{\sigma_{II}\alpha^2\Delta x_I}{k_I k_{II}}\overline{T_i}^2 - \frac{\sigma_{II}\alpha\Delta x_I\Delta x_{II}}{2k_I k_{II}}\overline{T_i}\,\overline{E_{i-1/2}}}{\frac{\Delta x_I}{k_I} + \frac{\Delta x_{II}}{k_{II}} + \frac{\sigma_{II}\alpha^2\Delta x_I}{k_I k_{II}}\overline{T_i}} \tag{2.43}$$

and the quadratic solution is:

$$T_{i-1/2} = -\frac{A - \sqrt{A^2 + 16\Delta x_I^2 k_{II}\alpha^2\overline{T_i} + 16\Delta x_I\Delta x_{II}\sigma_{II}\alpha^2 k_I\overline{T_{i-1}}}}{4\Delta x_I\sigma_{II}\alpha^2} \tag{2.44}$$

where

$$A = 2\Delta x_{II}k_I + 2\Delta x_I k_{II} - 2\Delta x_I\sigma_{II}\alpha^2\overline{T_i} + \sigma_{II}\alpha\Delta x_I\Delta x_{II}E_{i-1/2} \tag{2.45}$$

As can be seen, the solution to the quadratic equation is a very complicated expression, and for our model we choose to use the linear expression for $T_{i-1/2}$. The difference was tested using the code and found to be negligible.

Thus, the choice of $T_{i-1/2}$ made in equation (2.43) satisfies flux balance at the boundary between the heat equation and thermoelectric subdomains. The discretized expressions for $\frac{\partial T}{\partial x}$ on either side of the boundary are then:

$$\left(\frac{\partial T}{\partial x}\right)_l = \frac{T_{i-1/2} - \overline{T_{i-1}}}{\Delta x_l/2} \tag{2.46}$$

$$\left(\frac{\partial T}{\partial x}\right)_r = \frac{\overline{T_i} - T_{i-1/2}}{\Delta x_r/2} \tag{2.47}$$

where $T_{i-1/2}$ takes the value in equation (2.43). Something should be said about using this much more complicated expression instead of ignoring the additional thermoelectric terms and using the simple expression for $(\partial T/\partial x)_{i-1/2}$ from the heat equation flux balance on both sides of the boundary. Not including the exact expression derived from flux balance means that one is effectively introducing flux at the boundary which wouldn't be there naturally. This effect increases with the difference in the thermal conductivity across a boundary.

2.10 Boundary B, left side element

This section contains the discretization for the heat equation (equation (2.48)) in the mesh element on the left side of boundary B. A similar process can be used to derive the expression for the heat equation in the mesh element on the right side of boundary C.

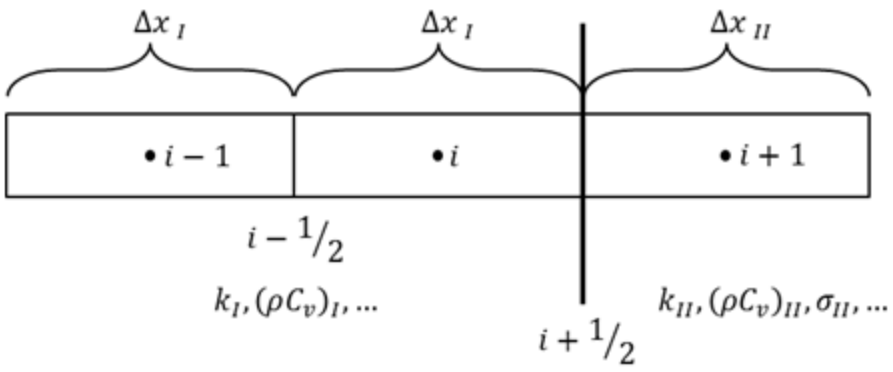

Figure 2.9: Boundary B (Left)

$$\rho C_v \frac{\partial T}{\partial t} = \frac{\partial}{\partial x}\left(k \frac{\partial T}{\partial x}\right) \tag{2.48}$$

$$\frac{1}{\Delta x_I}\int_{i-1/2}^{i+1/2} \rho C_v \frac{\partial T}{\partial t}\, dx = \frac{1}{\Delta x_I}\int_{i-1/2}^{i+1/2} \frac{\partial}{\partial x}\left(k \frac{\partial T}{\partial x}\right) dx \tag{2.49}$$

$$(\rho C_v)_I \frac{\partial \overline{T_i}}{\partial t} = \frac{k}{\Delta x_I}\left[\left(\frac{\partial T}{\partial x}\right)_{i+1/2} - \left(\frac{\partial T}{\partial x}\right)_{i-1/2}\right] \tag{2.50}$$

Now it is straightforward to write an expression at $i + 1/2$ using the expressions derived for previously:

$$(\rho C_v)_I \frac{\partial \overline{T_i}}{\partial t} = \frac{1}{\Delta x_I}\left[\frac{\frac{\frac{\Delta x_{II}}{k_{II}}\overline{T_I} + \frac{\Delta x_I}{k_I}\overline{T_{i+1}} + \frac{\sigma_{II}\alpha^2 \Delta x_I}{k_I k_{II}}\overline{T_{i+1}}^2 - \frac{\sigma_{II}\alpha \Delta x_I \Delta x_{II}}{2k_I k_{II}}\overline{T_{i+1}}\,\overline{E_{i+1/2}}}{\frac{\Delta x_I}{k_I} + \frac{\Delta x_{II}}{k_{II}} + \frac{\sigma_{II}\alpha^2 \Delta x_I}{k_I k_{II}}\overline{T_{i+1}}} - \overline{T_i}}{\Delta x_I / 2k_I} - \frac{\overline{T_i} - \overline{T_{i-1}}}{\Delta x_I / k_I}\right] \tag{2.51}$$

2.11 Boundary B, right side element

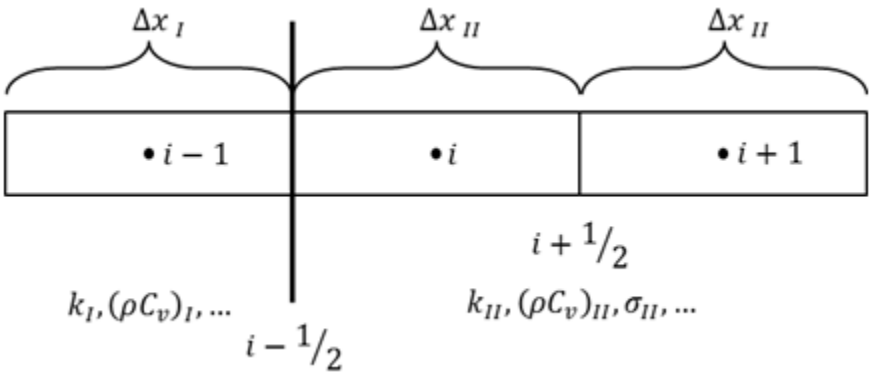

Figure 2.10: Boundary B (Right)

The derivations for the thermoelectric equations at the leftmost and rightmost elements in subdomain II begin exactly like equations (2.12) to (2.17), except now the value for $E_{i-1/2}$ is simply $\overline{E_{i-1/2}}$ since we have chosen to add an additional equation for it, and the values solved for previously for $T_{i-1/2}$ and $\left(\frac{\partial T}{\partial x}\right)_{i-1/2}$ can now be used where they are required. The resulting expressions are extremely long if displayed in full and can be easily written from equations (2.16), (2.17), (2.43) and (2.47) so we will omit them here.

2.12 Initial Conditions

For a best guess at the solution, we turn to the heat and current equations without the additional thermoelectric terms. If $\overline{T_1}$ is the temperature at the first mesh (the one closest to boundary A), $\overline{T_{N_{high}}}$ is the temperature at the left side of B, $\overline{T_{N_{high}+N}}$ is the temperature at the right side of C, $\overline{T_{N_{high}+N+N_{low}}}$ is the temperature at D, $\overline{E_B}$ and $\overline{E_C}$ are the electric fields at B and C respectively and $\overline{E_1}$ through $\overline{E_N}$ are the electric fields on the mesh nodes, then:

$$\overline{T_i} = T_{amb} + q_0 \left(N_{high} + N + N_{low} - i + \frac{1}{2} \right) \frac{\Delta x_{III}}{k_{III}} \quad for \quad N_{high}+N+1 \leq i \leq N_{high}+N+N_{low} \tag{2.52}$$

$$\overline{T_i} = \overline{T_{N_{high}+N+1}} + q_0 \left(\frac{\Delta x_{II}}{2k_{II}} + \frac{\Delta x_{III}}{2k_{III}} \right) + q_0 \left(N_{high} + N - i \right) \frac{\Delta x_{II}}{k_{II}} \quad for \quad N_{high}+1 \leq i \leq N_{high}+N \tag{2.53}$$

$$\overline{T_i} = \overline{T_{N_{high}+1}} + q_0 \left(\frac{\Delta x_{II}}{2k_{II}} + \frac{\Delta x_I}{2k_I} \right) + q_0 \left(N_{high} - i \right) \frac{\Delta x_I}{k_I} \quad for \quad 1 \leq i \leq N_{high} \tag{2.54}$$

$$\overline{E_B} = \overline{E_C} = \overline{E_i} = \frac{J_0}{\sigma_{II}} \quad for \quad 1 \leq i \leq N \tag{2.55}$$

Note that the final approximation, for E, is poor when J_0 is small , since when the forced current is low most of the electric field will be from the thermoelectric terms which are omitted in (2.55).

2.13 Derivation of Equivalent Circuit

The first step in developing an equivalent circuit model is to convert the conductivities and other material properties in the equations into circuit quantities, such as resistance and capacitance. Take the discretized TE equations in the bulk as an example:

$$\begin{aligned} \rho C_v \frac{\partial \overline{T_i}}{\partial t} = {} & \sigma \overline{E_i}^2 - \sigma \overline{\alpha}_i \overline{E_i} \frac{\overline{T_{i+1}} - \overline{T_{i-1}}}{2\Delta x} + \frac{k}{\Delta x} \left[\frac{\overline{T_{i+1}} - 2\overline{T_i} + \overline{T_{i-1}}}{\Delta x} \right] \\ & + \frac{\sigma \overline{\alpha_i}^2}{\Delta x} \left[\frac{\overline{T_{i+1}} + \overline{T_i}}{2} \frac{\overline{T_{i+1}} - \overline{T_i}}{\Delta x} - \frac{\overline{T_i} + \overline{T_{i-1}}}{2} \frac{\overline{T_i} - \overline{T_{i-1}}}{\Delta x} \right] \\ & - \frac{\sigma \overline{\alpha_i}}{\Delta x} \left[\frac{\overline{T_{i+1}} + \overline{T_i}}{2} \frac{\overline{E_{i+1}} + \overline{E_i}}{2} - \frac{\overline{T_i} + \overline{T_{i-1}}}{2} \frac{\overline{E_i} + \overline{E_{i-1}}}{2} \right] \end{aligned} \tag{2.56}$$

$$\epsilon \frac{\partial \overline{E_i}}{\partial t} = J_0 - \sigma \overline{E_i} + \sigma \overline{\alpha_i} \frac{T_{i+1} - T_{i-1}}{2\Delta x} \tag{2.57}$$

First, the electric field must be written in terms of voltage. To do this, we make use of the following definition:

$$W(x,t) = E\Delta x \tag{2.58}$$

in order to introduce W, a quantity of convenience which is the voltage difference across the element. This Δx represents the same Δx as the others in the two equations since the electric field being discussed is measured across the mesh element. The equations

become:

$$\rho C_v \frac{\partial \overline{T_i}}{\partial t} = \frac{\sigma \overline{W_i}^2}{\Delta x^2} - \sigma \overline{\alpha_i} \frac{\overline{W_i}}{\Delta x} \frac{\overline{T_{i+1}} - \overline{T_{i-1}}}{2\Delta x} + \frac{k}{\Delta x} \left[\frac{\overline{T_{i+1}} - 2\overline{T_i} + \overline{T_{i-1}}}{\Delta x} \right] + \frac{\sigma \overline{\alpha_i}^2}{\Delta x} \left[\frac{\overline{T_{i+1}} + \overline{T_i}}{2} \frac{\overline{T_{i+1}} - \overline{T_i}}{\Delta x} - \frac{\overline{T_i} + \overline{T_{i-1}}}{2} \frac{\overline{T_i} - \overline{T_{i-1}}}{\Delta x} \right] - \frac{\sigma \overline{\alpha_i}}{\Delta x} \left[\frac{\overline{T_{i+1}} + \overline{T_i}}{2} \frac{\overline{W_{i+1}} + \overline{W_i}}{2\Delta x} - \frac{\overline{T_i} + \overline{T_{i-1}}}{2} \frac{\overline{W_i} + \overline{W_{i-1}}}{2\Delta x} \right] \tag{2.59}$$

$$\frac{\epsilon}{\Delta x} \frac{\partial \overline{W_i}}{\partial t} = J_0 - \frac{\sigma \overline{W_i}}{\Delta x} + \sigma \overline{\alpha_i} \frac{T_{i+1} - T_{i-1}}{2\Delta x} \tag{2.60}$$

Now multiply the temperature equation by $A\Delta x$ and multiply the voltage equation by A to obtain:

$$C_{th} \frac{\partial \overline{T_i}}{\partial t} = \frac{\overline{W_i}^2}{\Delta R_e} - \overline{\alpha_i} \frac{\overline{W_i}}{\Delta R_e} \frac{\overline{T_{i+1}} - \overline{T_{i-1}}}{2} + \frac{1}{\Delta R_{th}} \left(\overline{T_{i+1}} - 2\overline{T_i} + \overline{T_{i-1}} \right) + \frac{\overline{\alpha_i}^2}{2\Delta R_e} \left(\overline{T_{i+1}}^2 - 2\overline{T_i}^2 + \overline{T_{i-1}}^2 \right) - \frac{\overline{\alpha_i}}{4\Delta R_e} \left[\left(\overline{T_{i+1}} + \overline{T_i} \right) \left(\overline{W_{i+1}} + \overline{W_i} \right) - \left(\overline{T_i} + \overline{T_{i-1}} \right) \left(\overline{W_i} + \overline{W_{i-1}} \right) \right] \tag{2.61}$$

$$C_e \frac{\partial \overline{W_i}}{\partial t} = I_0 - \frac{\overline{W_i}}{\Delta R_e} + \overline{\alpha_i} \frac{T_{i+1} - T_{i-1}}{2\Delta R_e} \tag{2.62}$$

where the following substitutions have been made:

$$C_{th} = A\Delta x \rho C_v \tag{2.63}$$

$$\Delta R_{th} = \frac{\Delta x}{kA} \tag{2.64}$$

$$\Delta R_e = \frac{\Delta x}{\sigma A} \tag{2.65}$$

$$C_e = \frac{A\epsilon}{\Delta x} \tag{2.66}$$

$$I_0 = AJ_0 \tag{2.67}$$

The terms in the equations can be thought of as currents into a node. The diffusive flux and capacitive terms become resistors and capacitors, respectively, and any terms which cannot be represented by a passive circuit element can be represented by nonlinear controlled current sources. The result is two coupled distributed circuits, one for the electrical equation and one for the thermal equation. The simpler electrical circuit is shown in figure 2.11:

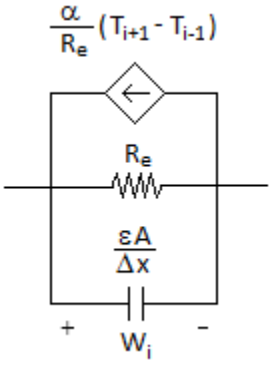

Figure 2.11: Equivalent Circuit Element (Electrical)

For the thermal circuit, one can lump all of the nonlinear thermoelectric terms into a single current source going into the node, as shown in figure 2.12, or alternatively one can separate the volume sources from the flux terms in the integral formulation, as shown in figure 2.13. These two methods are mathematically equivalent in that the node equations written out in either case will be identical. The first option is slightly easier to implement since all of the terms are in a single current source while the second is more physically intuitive.

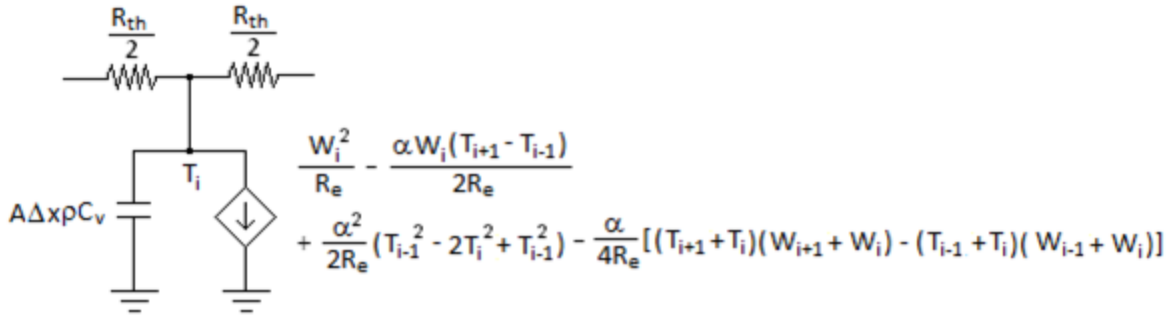

Figure 2.12: Equivalent Circuit Element (Thermal)

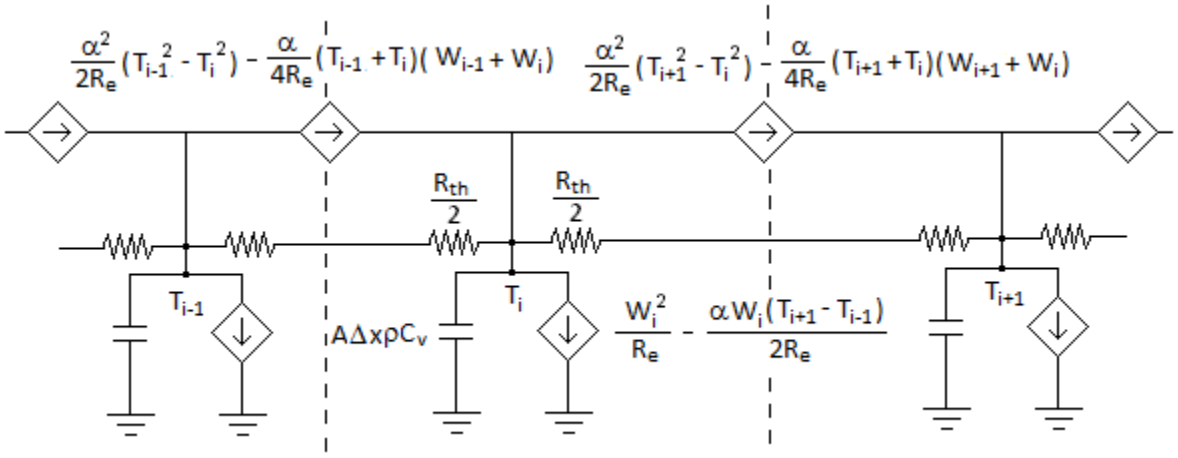

Figure 2.13: Equivalent Circuit Element (Thermal, Alternative)

As mentioned previously, a circuit model can be used as a quick and accurate tool for simulating systems of equations given that the circuit is an exact representation of the underlying equations. However, while it is possible for our equivalent circuit model to be created in a commercial circuit simulator, it is more practical to numerically solve the system of ODEs directly. This is due to the difficulty of circuit simulators to simulate current sources which are arbitrary functions of values measured elsewhere in the circuit. Another restriction stemming from circuit software is its inability to model distributed networks consisting of non-standard elements (i.e. more than just an RC network). The circuit model developed in this chapter, being relatively simple, is generally more useful

as a conceptualization/visualization tool.

2.14 Scaling

Since the thermoelectric model was developed for a single piece of thermoelectric material, it is important to discuss how it would scale when the materials are arranged as a PN thermocouple, and furthermore with M thermocouples electrically in series and thermally in parallel, as is the case in commercial thermoelectric modules. First, it is possible to use the one-dimensional model to solve for a PN couple by replacing the transport parameters with their combined values (i.e. $\alpha = \alpha_p - \alpha_n$, $1/\sigma = 1/\sigma_p + 1\sigma_n$, $k = k_p + k_n$, etc.). This is done because in such a configuration, the total length is altered for the electrical equation while the area is altered for the thermal equation and so it doesn't make sense to alter the subdomain lengths of the two equations separately. This type of approximation makes the assumption that the transport coefficients in the P and N legs of the thermocouple are nearly equal so that the problem can still be treated as one-dimensional.

The approach for two elements can be generalized to the case with M elements. For the electrical equation, since M elements are now in series, the total length is multiplied by M while the cross-sectional area stays the same. For the thermal circuit, the total cross-sectional area is multiplied by M while the length stays constant. This has the effect of setting $1/\sigma_{tot} = M/\sigma$, $k_{tot} = Mk$ and $\alpha_{tot} = M\alpha$, etc.

In applications where scaling needs to occur, it is probably easiest to use resistances and capacitances instead of conductivities. Using resistances, the physical area and length are lumped into one term and so all one needs to worry about is that the total resistance is modified by M and the resistance of each discretized element is the total resistance divided by M.

2.15 Simulation

The finite volume model was tested using Matlab's ODE solver. A slightly modified version of the equations was used in the code (See Appendix F for Matlab code) due to the fact that thermal and electrical resistances (R) and capacitances (C) were measured instead of conductivities (k, σ) and capacities (C_v, ϵ), which were used in the original discretization. As an example, the equations used to represent the bulk in the MATLAB code are identical to equations (2.61) and (2.62).

Matlab's ode23 ODE solver (one of Matlab's implementations of an explicit Runge-Kutta method) was used to solve the system of ODE's. The material properties used in the code were measured using the experimental apparatus and heat capacity calculations were made based on weight. The Seebeck coefficient, α, is implemented in the code as a third-order Lagrange polynomial approximation with constant values above and below the highest and lowest measured temperature. Figure 2.14 shows a comparison between the measured and simulated results starting at room temperature with an input power of 20 Watts. In this case the initial conditions were room temperature and zero voltage at each node in the system. The two simulated curves are for the finite volume model developed in this chapter, as well as for a simple model based on equations 2.1 and 2.1 with a simplified linear model for each subdomain.

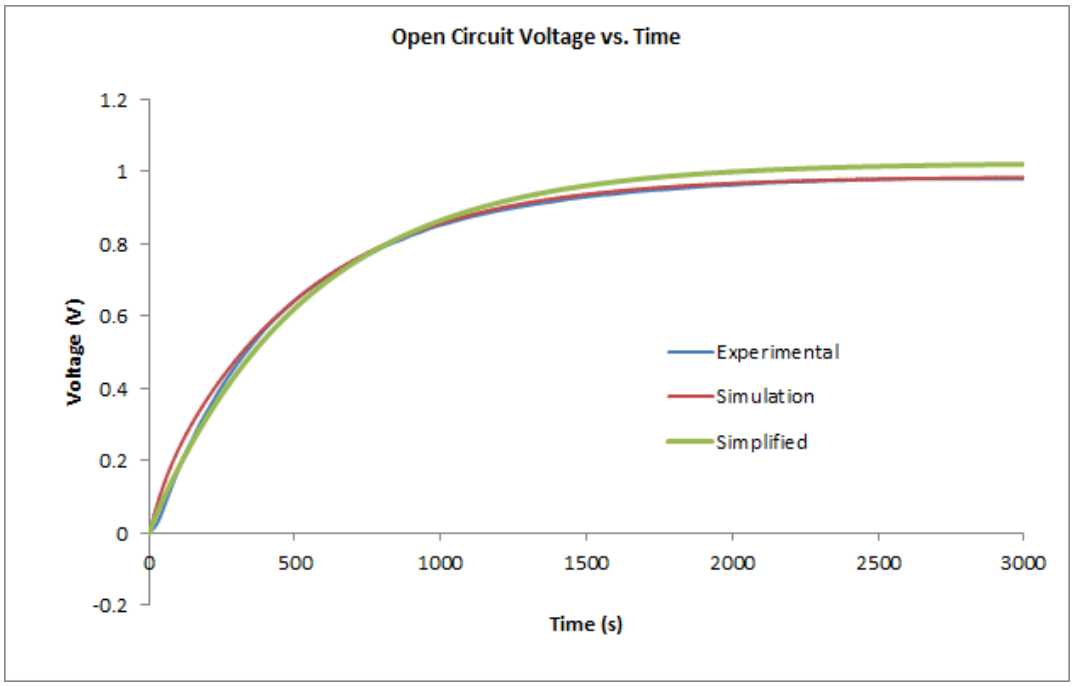

Figure 2.14: Open Circuit Voltage vs. Time

Good agreement during the transient and steady state are seen between all three curves. Since most of the time-dependent behavior of the experimental system is due to the heat capacity of the heat sinks, the simple model predicts the transient behavior of the system well. However, since the simple model uses a constant value for alpha, it will produce steady-state errors for voltage unless the value for α which happens to produce the correct result is used. The following table shows the steady state voltage and computation times for the finite volume model for different mesh refinements:

Meshes	Computation Time (s)	V
Simple (3)	0.3	1.02
6	35.5	0.9667
12	42.2	0.9769
18	42.9	0.9805
24	46.1	0.9823
30	49.3	0.9834
60	74.6	0.9854
62	84.3	0.9854

For an overview of the experimental apparatus, refer to Appendix E and for the Matlab code, refer to Appendix F.

2.16 Summary

In this chapter, a finite volume model for a thermoelectric device was developed. Various existing models were evaluated and it was found that some were too simple and lacked important facets, such as time dependence and variable transport coefficients. In order to address these issues, a more thorough and mathematically rigorous approach was taken. The problem was restricted to one spatial dimension due to the symmetries present in most applications involving thermoelectric materials and discretized using a centre-differencing finite volume method. The domain was divided into three subdomains: the high side heat exchanger, the thermoelectric material and the low side heat exchanger. The discretization process was carried out for the corresponding equations on each of these subdomains: the heat exchanger subdomains contained the heat equation and the thermoelectric subdomains contained the coupled thermoelectric PDE's. Particular attention was paid to the internal boundaries, on which flux balance was applied to obtain the correct expressions for the boundary temperatures and voltages. Acceptable

approximations for the initial conditions for the system were chosen based on the ordinary heat and current equations. Using a thermal-electrical circuit analogy, an equivalent distributed circuit element was created of the non-boundary elements as a visualization tool. However, actually creating the model in many commercial circuit simulators is difficult due to their restrictions in creating dependent sources. Finally, a method to scale the model to multiple thermocouples was discussed.

Using Matlab, transient results from the model were compared to experimentally measured results and good agreement was observed.

Chapter 3

Case Study: Thermoelectric Heat Sink Design

3.1 Introduction

Power devices must be cooled in order to avoid damaging the semiconductor junction and risking device failure. The standard thermal management technique for high power devices involves a heat sink and some form of active cooling, which may be either air or liquid-based. In this chapter we investigate whether a thermoelectric device can be incorporated into a cooling system to keep the device cooled to specification while still generating power from waste heat. One possible application for such a device is in systems with high voltages where there are cost incentives against bringing in external voltages to power cooling systems and a self-contained cooling unit would be desirable.

To do this, we attempt to optimize the geometry of the heat sink to deliver maximum heat flux to a thermoelectric module while keeping the junction temperature of the power device below its maximum rated temperature. Furthermore, we explore the possibility of the power generated by the TE module being used to power a cooling fan, in order to have a completely self-contained cooling unit. The finite element simulation package

COMSOL is used extensively in the design process to optimize the geometry and validate our designs. We perform both static and transient heat transfer simulations to examine the steady state and start-up behavior of the system.

3.2 Design Constraints

Essentially the goal is to remove sufficient heat from the device so that it does not overheat, while retaining the largest temperature at the hot side of the TE module to generate power. There are two broad categories in terms of geometrical configurations: the thermoelectric module can either be thermally in series or in parallel with the main heat sink. Furthermore, flow conditions considered for the chosen geometry must include both forced convection for the steady state and natural convection for the start-up transient. The following constraints are required:

- Constraint 1: Maximum junction temperature of 125 C
- Constraint 2: Create the largest possible temperature difference across thermoelectric module given constraint 1
- Constraint 3: Thermal contact can only be made on one side of the device (usually the case for power devices)

3.3 Thermal Circuit

A thermally series configuration, as show in figure 3.1, is not feasible simply because, while it would provide the largest temperature difference across the thermoelectric module, the thermal resistance of the TE module is so large that efficient heat removal is impossible, even with forced convection.

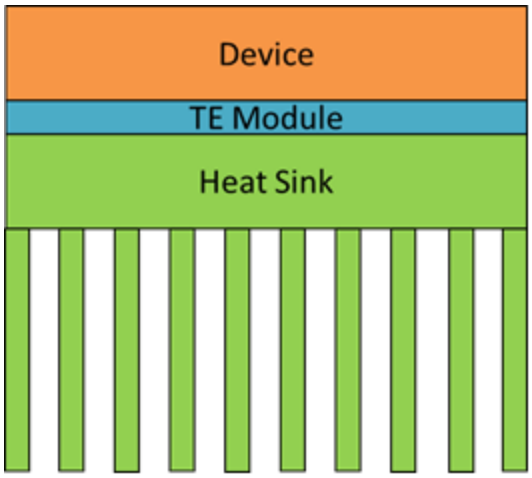

Figure 3.1: Thermally Series Configuration

This leaves a parallel configuration as the only alternative. Regardless of the exact geometry, the general simplified DC thermal circuit for any parallel configuration will have the same structure in steady state and is shown in figure 3.2.

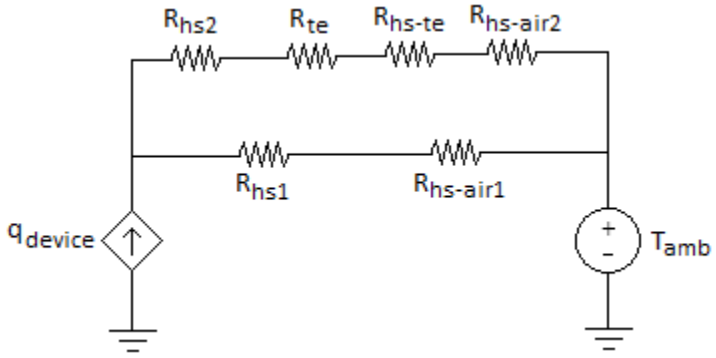

Figure 3.2: Simplified DC Thermal Circuit

In this DC thermal circuit, R_{te}, the thermoelectric module's thermal resistance, can be assumed to be much larger than the combined thermal resistance of the other branch, so that very little heat passes through the thermoelectric branch. R_{hs} depends on the geometry and heat sink material, while R_{hs-air} depends on the surface area of the fins and air speed in the forced convection case. We also assume that we have no control over R_{te}, since the surface area available for the TE module will necessarily be on the

order of the size of the device. With these assumptions, the original design constraints amount to a maximization of the high side temperature up to T_{junct} by increasing R_{hs1} and $R_{hs-air1}$ while minimizing the heat sink resistances in the top branch so that as much of the temperature difference as possible appears across R_{te}. We propose one possible configuration, shown in figure 3.3, which allows us to modify these parameters.

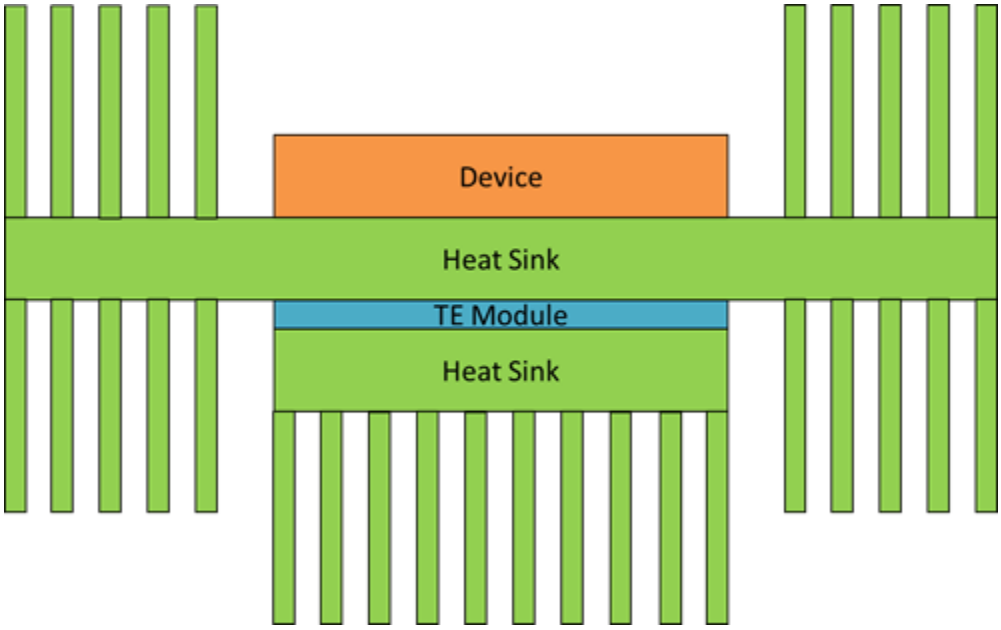

Figure 3.3: Thermally Parallel Configuration

In the proposed configuration, the TE module is placed at the hottest point of the heat sink, so that as long as constraint 1 is met, constraint 2 is also met. R_{hs-air} can be modified by changing the number of fins in the main heat sink and the thermoelectric heat sink, and R_{hs1} and R_{hs2} can be changed by altering the dimensions of the main heat sink.

3.4 FEM Simulation

Ultimately, the goal of designing this type of combined thermoelectric heat sink is to have the cooling fan powered by the thermoelectric module. In order to test the viability

of doing so, we have created a case study of the geometry in figure 3.3 for a hypothetical power electronics device based on the MBN1500E33 from Hitachi, a power IGBT with 2 kW of power dissipation.

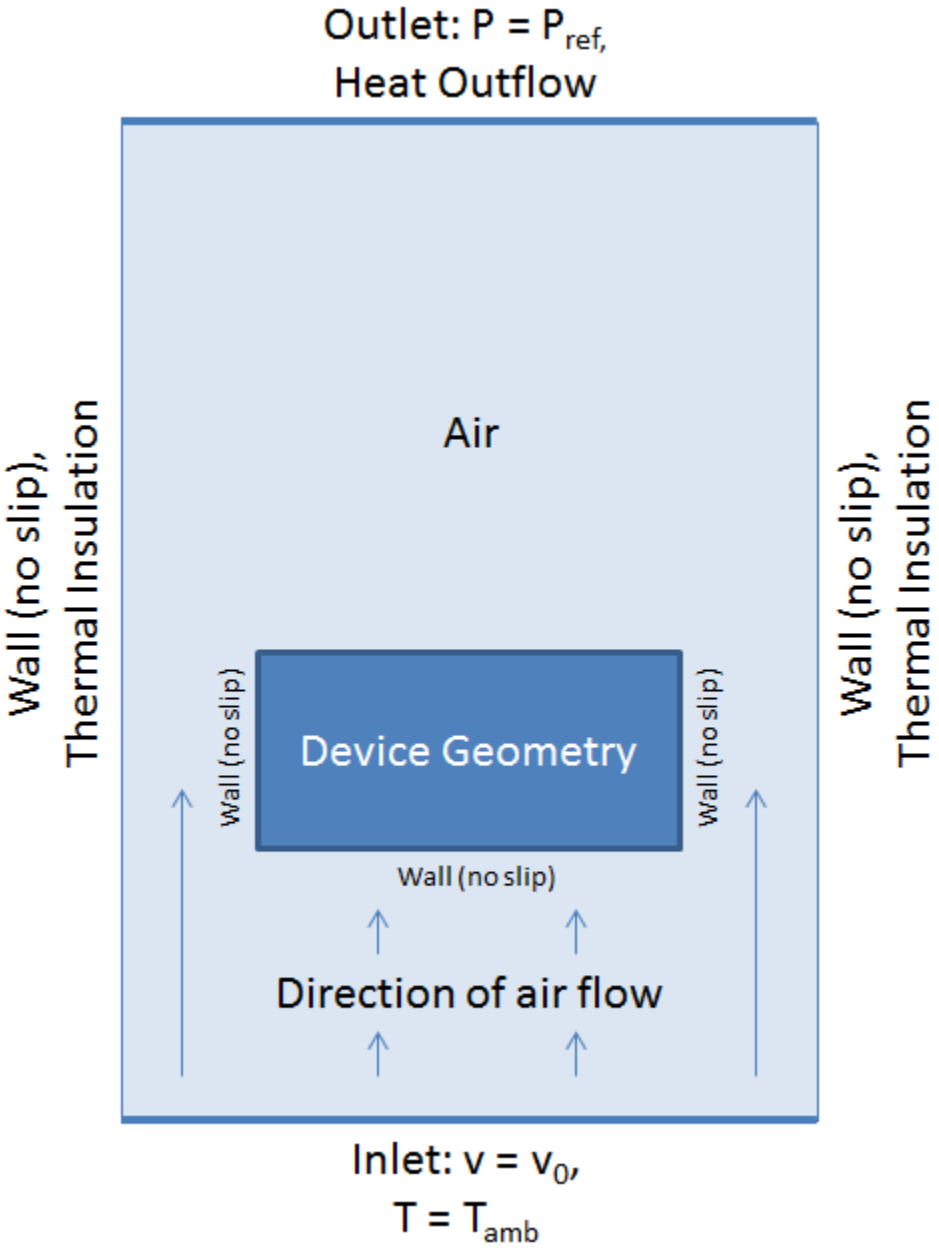

Figure 3.4: Boundary Conditions, Forced Convection

In the simulation, the device is a volumetric heat source producing 2000 W and the

thermoelectric module has the same length and width as the device, with a thickness of 3.4 mm (roughly the thickness of a commercial Peltier cooler). In accordance with the assumption that heat can only be removed from one side of the device, the top surface has a thermal insulation boundary condition. Figure 3.4 shows the boundary conditions for the steady-state forced convection simulations. The device is immersed in a box of air in which represents open space. The heat equation is solved on the solid and coupled to the incompressible Navier-Stokes equations on the fluid domain via continuity for heat and the no-slip condition for fluid flow. The no-slip boundary condition on walls is a common approximation made in computational fluid dynamics for low and intermediate velocities, and greatly simplifies the computation as long as the fins are not close enough together that boundary overlap effects occur. The inlet boundary conditions are constant temperature and velocity profile and the outlet boundary conditions are constant pressure and heat outflow. The heat outflow condition in COMSOL is identical to thermal insulation and states that the only heat transfer is by convection. The side walls of the fluid domain also have the thermal insulation condition and no-slip walls which, for a large enough box approximates a large open domain.

Figures 3.5 to 3.9 show the results of the forced convection simulations.

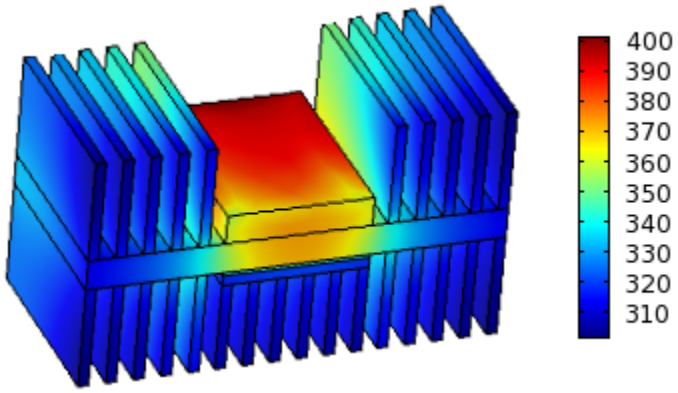

Figure 3.5: Surface Temperature, Forced Convection

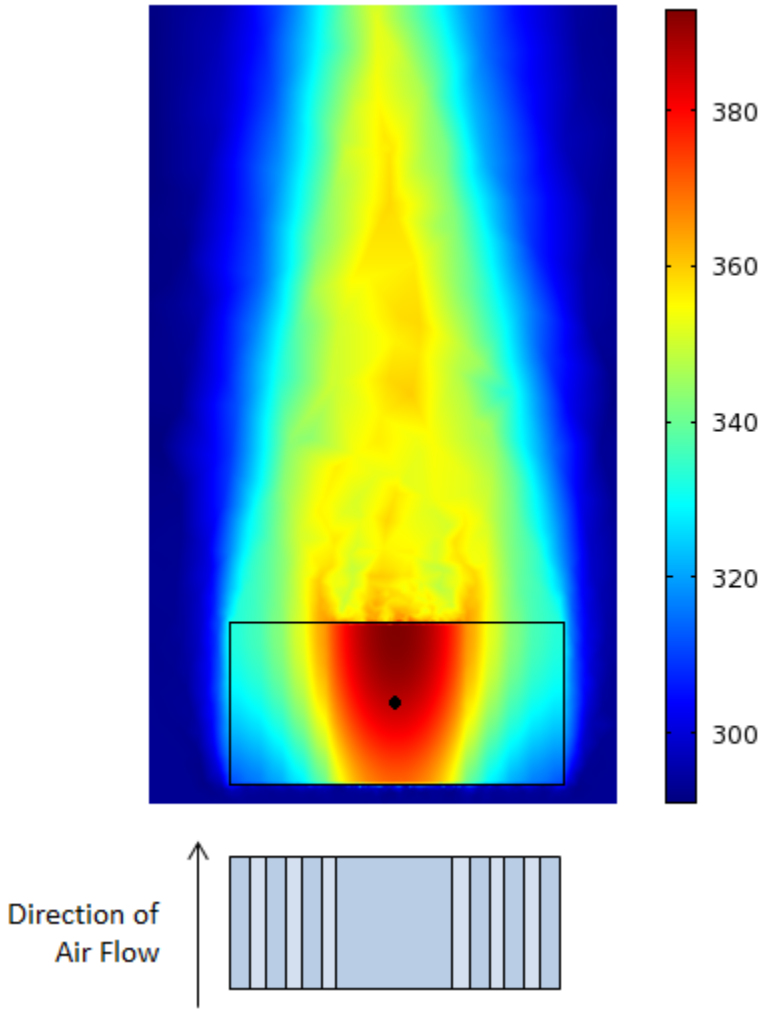

Figure 3.6: Cross Sectional Temperature, Forced Convection (Temperatures in Kelvin)

The rectangular outline in figure 3.6 represents the position of the device, and the point denotes the axis along which figure 3.7, the temperature profile, is plotted. The orientation of the in figure 3.6 is the same as in figure 3.4. In figure 3.7, the temperature profile goes linearly from $x = 0$ mm, the top of the IGBT to $x = 16$ mm, the tip of the thermoelectric heat sink's fins.

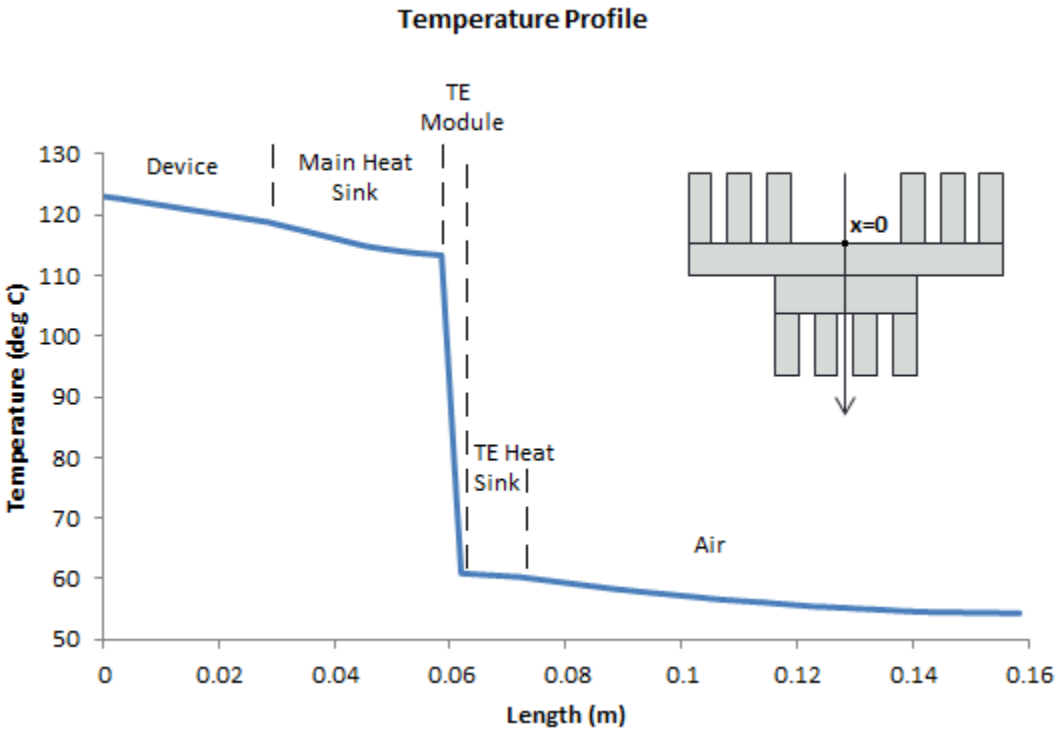

Figure 3.7: Temperature Profile, Forced Convection

With an inlet velocity of 2 m/s, we see a drop of approximately 60° C across the thermoelectric module in steady state, quite good considering the highest temperature in the system is just under 125 degrees. Integrating the heat flux into the TE module results in a value of 250 W. Assuming an average efficiency of 4% for the thermoelectric module, around 10 W of power will be recovered.

Integrating the pressure drop over the inlet and multiplying by the inlet velocity, we calculate the fan power required to cool the heat sink to be about 5 W. In theory then, it appears that by using an optimized geometry and with an efficient thermoelectric material, using the recovered heat to power the cooling fan in closed loop is possible, at least in steady state. A trade-off can be made between output power and fan speed (and hence, device temperature) since increasing fan speed lowers the average temperature of the system. Figures 3.8 and 3.9 show the total heat flux through the thermoelectric module and temperature, respectively, as functions of fan speed.

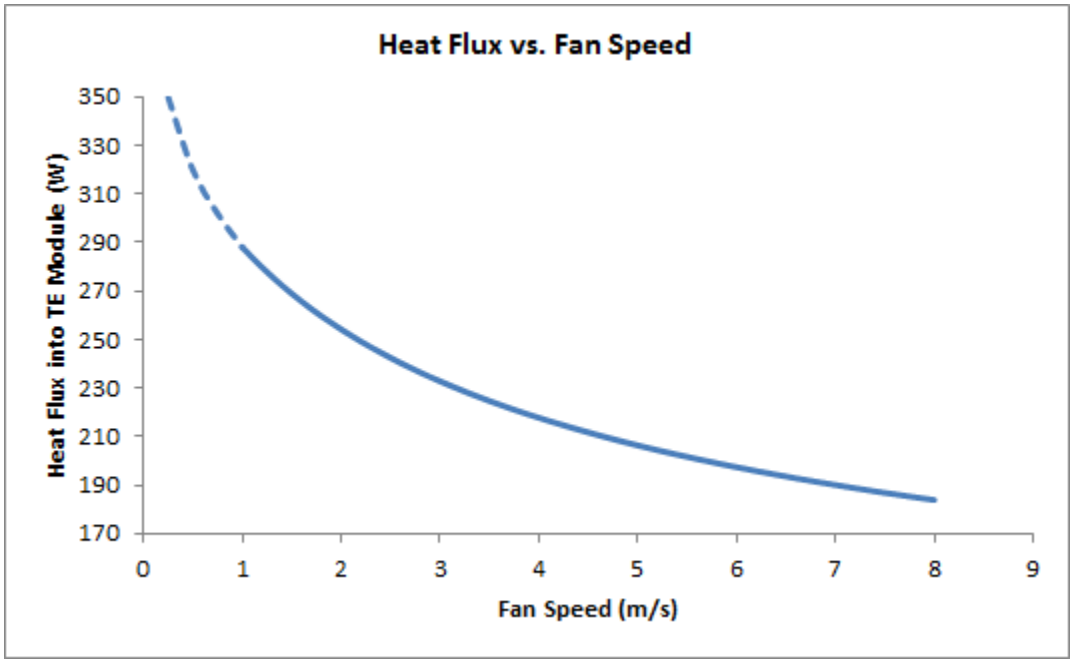

Figure 3.8: Heat Flux vs. Fan Speed

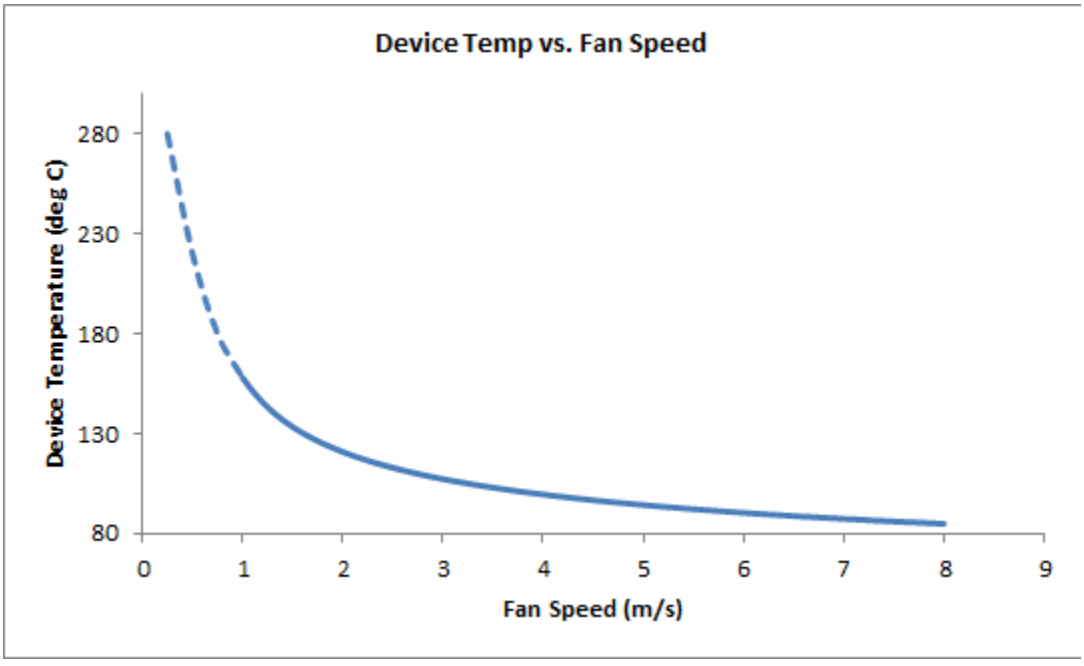

Figure 3.9: Device Temperature vs. Fan Speed

The heat flux-vs.-fan speed (Figure 3.8) and device temperature-vs.-fan speed (Figure 3.9) are extrapolated below 1 m/s due to the fact that the forced convection model does

not take into account natural convection. At low fan speeds the steady-state solution approaches a situation where temperature is uniform and no heat flows through either branch, which is unrealistic. If the fan power-vs.-fan speed characteristic is known, then the intersection between the fan power-vs.-fan speed and power generated-vs.-fan speed curves denotes the steady state operating point of the system without any control, as shown in figure 3.10.

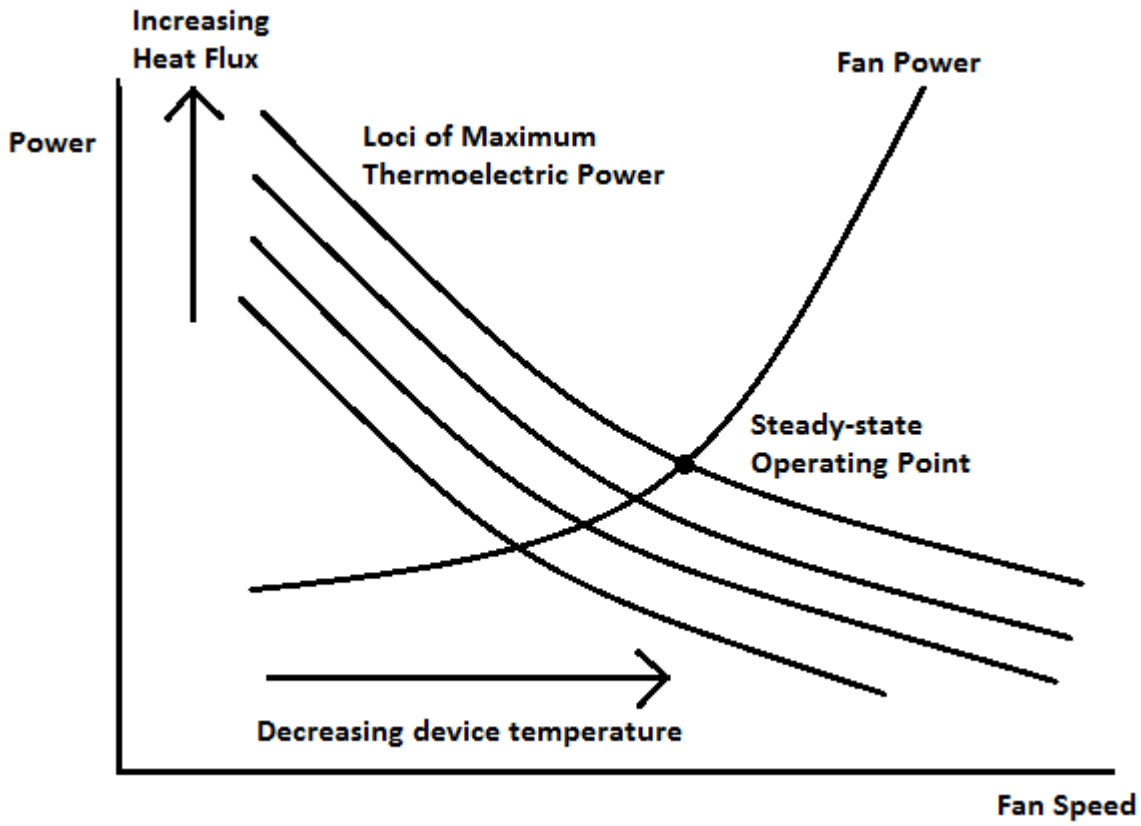

Figure 3.10: Operating Point

The locuses of maximum thermoelectric power represent the peak power points (refer to Figure **??**) as functions of input heat and fan speed, with reference to Figure 3.8, since the peak power generated will be a fixed percentage of the total heat flux through the thermoelectric leg of the geometry. The point shown in figure 3.10 is the operating point with the least available power output. Therefore, any operating point to the left of the

steady-state operating point along the fan power curve is possible with the appropriate control system, trading power output for device temperature while generating excess power. A block diagram of one possible implementation of a control system is shown in figure 3.11.

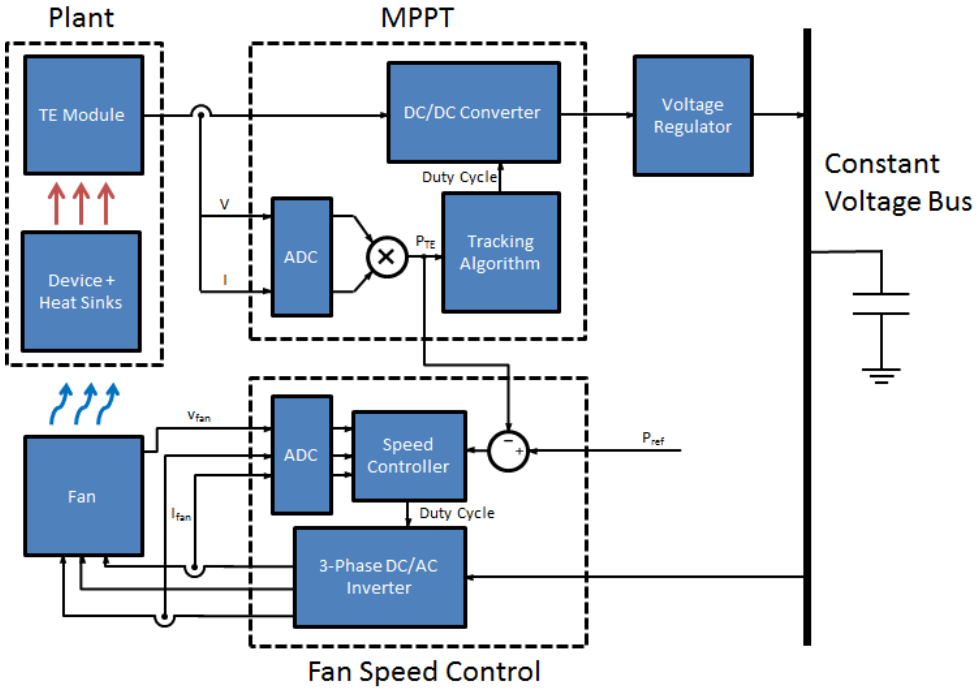

Figure 3.11: Example Control System

The components of the control system in figure 3.11 are:

- Plant: The plant includes the heat sinks and thermoelectric module, which may be obtained using the appropriate model, for instance the one developed in this paper.
- Maximum power point tracker (MPPT): A controller which measures the input voltage and current and alters the duty cycle of a dc/dc converter to maintain the instantaneous power VI at a maximum. This ensures that the power being output by the TE module remains on the locus of peak power points.
- Voltage Regulator and Bus: Creates a constant voltage bus to power the fan and

to distribute excess power if the fan is not taking 100% of the power generated.

- Fan Controller: Measures fan current and speed in order to regulate fan speed. The fan speed command can be (1) set based on the difference between the measured thermoelectric power and a reference power, (2) set at a constant value or (3) be allowed to reach the steady state operating point. The fan controller then sends the PWM signals to the inverter which powers the fan.

- Fan: A synchronous motor which cools the device and heat sinks.

The final thing to consider is the start-up behaviour of such a coupled system. Since we have already designed for the system to have the maximum allowed junction temperature in order to recover the largest amount of energy, having the system start in natural convection will shoot T_{junct} past 125 degrees C. Assuming the fan gets enough power to turn on at exactly 125 degrees, it is of interest to simulate exactly how much higher the temperature rises and for how long. For this purpose we designed another simulation with natural convection conditions, ran that simulation until T_{junct} reached 125 degrees, and used the state at that point as the initial conditions for a forced convection simulation. The result is shown in figure 3.12.

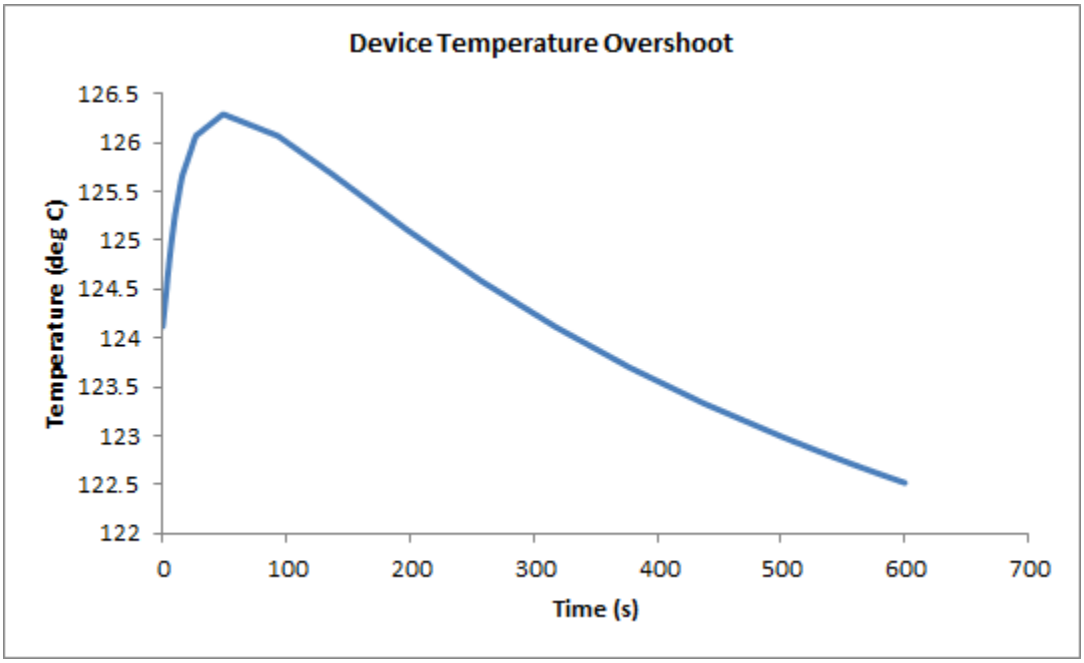

Figure 3.12: Temperature Overshoot

The results of the simulation show that for our test case, the temperature overshoot is on the order of a few degrees over a time scale of tens of seconds. The percent overshoot would depend on the geometry of the heat sink and the amount of heat being generated by the device, but these results show any transient temperature rise during start-up is limited in both magnitude and duration.

3.5 Summary

The steady state and transient behavior of the sample design was investigated, and it was found that a steady state solution where a fan was being driven by power generated from waste heat was theoretically possible, and that the temperature overshoot associated with startup was relatively minor. A possible control structure for the system was also considered.

Chapter 4

Conclusion

Thermoelectricity is a promising method of harvesting low-grade waste heat in applications where traditional methods are impractical. Applications of thermoelectric generators are generally limited by their low efficiency, which is improving as new materials and structures are discovered. In this work, a finite volume based one dimensional model of thermoelectric generators was made. The model is time-dependent and includes temperature-dependent coefficients as well as the high side and low side heat sinks. The model, simulated using Matlab, was shown to accurately reproduce experimental measurements of the open circuit voltage of a commercial module.

Separately, in order to investigate whether a thermoelectric module can be integrated into a cooling system for a power semiconductor, a heat-sink/thermoelectric generator assembly was designed and simulated in COMSOL. It was found that, given high enough power, the thermoelectric generator was able to harvest enough heat to power a cooling fan and still keep the junction temperature below the maximum rated junction temperature. Furthermore, it was found that the temperature overshoot in the system during fan startup is fairly insignificant.

4.1 Contributions

The main contribution from this work is a new finite volume model of thermoelectric devices based on the physics of the thermoelectric effect. Though for a one-dimensional model the various discretization schemes are closely related, the finite volume method was used because it is more intuitive from a physical perspective. This model can be used to very exactly predict the transient and steady-state behaviour of a complete thermoelectric system including heat sinks, given the material properties are known. Furthermore, the equivalent circuit representation of the model was developed for visualization purposes.

4.2 Future Work

Directions for further research along the same lines include possible ways to expand the finite volume model, perhaps into higher dimensions or to include more phenomena such as contact resistance. Also, it would be interesting to perform an experimental verification of the theoretical results in Chapter 4 in order to see how accurate the results of the heat transfer simulations are.

Appendix A

Derivation of the Transport Equations

A.1 Carrier Transport in Solids

The function $f(t, \vec{r}, \vec{p})$ is defined as the distribution function in one particle phase space; it is the probability density of systems having generalized position and momentum coordinates $(\vec{r}, \vec{p})$. Thus, $f(t, \vec{r}, \vec{p})\, d^3r d^3p$ is the number of systems within the volume $d^3r d^3p$ in phase space. The time evolution of $f(t, \vec{r}, \vec{p})$ is governed by the Boltzmann equation which is based on the continuity of the distribution function in phase space, with interactions between particles lumped into a collision term:

$$\frac{\partial f}{\partial t} + \frac{\partial \vec{r}}{\partial t} \cdot \nabla_r f + \frac{\partial \vec{p}}{\partial t} \cdot \nabla_p f = \left(\frac{\partial f}{\partial t} \right)_{coll} \tag{A.1}$$

where

$$\frac{\partial \vec{r}}{\partial t} = \frac{\partial x}{\partial t}\hat{x} + \frac{\partial y}{\partial t}\hat{y} + \frac{\partial z}{\partial t}\hat{z} \tag{A.2}$$

$$\nabla_p = \frac{\partial}{\partial p_x}\hat{p}_x + \frac{\partial}{\partial p_y}\hat{p}_y + \frac{\partial}{\partial p_y}\hat{p}_z \tag{A.3}$$

and

$$\left(\frac{\partial f}{\partial t}\right)_{coll} = \sum_{\vec{p'}} S\left(\vec{p},\vec{p'}\right) f\left(\vec{p}\right)\left[1 - f\left(\vec{p'}\right)\right] - \sum_{\vec{p'}} S\left(\vec{p'},\vec{p}\right) f\left(\vec{p'}\right)\left[1 - f\left(\vec{p}\right)\right] \quad \text{(A.4)}$$

is the sum of the collision probabilities into and out of state $\vec{p}$. In equation (A.4), $S\left(\vec{p},\vec{p'}\right)$ is the transition probability from $\vec{p}$ to $\vec{p'}$, $f\left(\vec{p}\right)$ is the probability that state $\vec{p}$ is occupied and $\left[1 - f\left(\vec{p'}\right)\right]$ is the probability that state $\vec{p'}$ is unoccupied. Several approximations can be made at this point to allow an analytic solution. The first and most drastic is the *relaxation time approximation*, which states that:

$$\left(\frac{\partial f}{\partial t}\right)_{coll} \approx -\frac{f - f_0}{\tau} \quad \text{(A.5)}$$

Where τ is the relaxation time and f_0 is the equilibrium or unperturbed distribution function. This approximation is a simplification of scattering, which allows the perturbed and unperturbed functions to be related. The relaxation time approximation is widely used because it makes the Boltzmann equation much easier to solve compared to attempting a full quantum mechanical treatment. However, the relaxation time approximation may only be applied when certain very stringent criteria are met. In order for the scattering rates to be encapsulated in the relaxation time, (1) τ is assumed not to be a function of energy and (2) the energy gained or lost by electrons in non-elastic collisions must be small compared to the electron's original energy. Under the relaxation time approximation, equation (A.1) can be rewritten as:

$$\frac{\partial f}{\partial t} + \vec{v}\cdot\nabla_r f + \frac{\vec{F}}{m}\cdot\nabla_v f = -\frac{f - f_0}{\tau} \quad \text{(A.6)}$$

where $\vec{v} = \partial\vec{r}/\partial t = \vec{p}/m$ and $F = \partial\vec{p}/\partial t$ (m is the effective mass of the particle). Equation (A.6) can be further rewritten in terms of f_0 and the difference between f and f_0:

$$\frac{\partial\left(f - f_0\right)}{\partial t} + \frac{\partial f_0}{\partial t} + \vec{v}\cdot\nabla_r f_0 + \vec{v}\cdot\nabla_r\left(f - f_0\right) + \frac{\vec{F}}{m}\cdot\nabla_v f_0 + \frac{\vec{F}}{m}\cdot\nabla_v\left(f - f_0\right) = -\frac{f - f_0}{\tau} \quad \text{(A.7)}$$

At this point some further approximations can be made in order to linearize the Boltzmann equation:

1. The deviation of the distribution function from equilibrium is small, i.e. $|f - f_0| \ll f_0$
2. The gradient of $f - f_0$ is small compared to the gradient of f_0
3. Changes in the external fields happen much slower than τ (transient terms are negligible)

Using these approximations, many of the terms in the previous equation can be neglected and f can be written as:

$$f = f_0 - \tau \left(\vec{v} \cdot \nabla_r f_0 + \frac{\vec{F}}{m} \cdot \nabla_v f_0 \right) \tag{A.8}$$

This approximation process takes into account only the first order expansion of f (where f_0 is the zeroth order term) and neglects any higher order terms. Using this expression it is now possible to derive analytical expressions for the flux of charge and heat.

Now the distribution function f is known, a particle in a particular state with wavevector $\vec{k}$ carries a charge flux J_e and J_q and heat flux equal to:

$$J_e = qv\left(\vec{k}\right) D\left(E, \vec{k}\right) f \tag{A.9}$$

$$J_q = Ev\left(\vec{k}\right) D\left(E, \vec{k}\right) f \tag{A.10}$$

where q is the particle's charge, v is the particle's group velocity, and $D(E)$ is the differential density of states, defined as the density of states $g(E)$ per solid angle Ω. In isotropic media, the differential density of states does not depend on angular direction and is equal to $g(E)/4\pi$, or the density of states divided by the solid angle of a sphere.

For convenience, only the one-dimensional gradients in the x-direction will be considered. θ is defined as the angle between $\vec{k}$ and the x-axis and ϕ is defined as the angle between the projection of $\vec{k}$ onto the y-z plane and the y-axis. Using this geometry, the

x-component of the velocity can be written simply as $v_x = v\cos\theta$ and the differential solid angle as $d\Omega = \sin\theta d\theta d\phi$.

A.2 Solution to the Linearized Boltzmann Equation under the Relaxation Time Approximation

In semiconductors, the equilibrium distribution function for electrons and holes is known to be the Fermi-Dirac distribution:

$$f_0 = f\left(E, E_f, t\right) = \frac{1}{\exp\frac{E-E_f}{kT}+1} \tag{A.11}$$

where both E and E_F are measured from the bottom of the conduction band for electrons and from the top of the valence band for holes.

For thermoelectric phenomena, the semiconductor is under both an electric field and a temperature gradient simultaneously. This implies that both the Fermi level and temperature are functions of position. Therefore, f can be written as:

$$\begin{aligned} f &= f_0 - \tau\left(v_x\frac{\partial f_0}{\partial x} - \frac{e\mathcal{E}}{m}\frac{\partial f_0}{\partial v_x}\right) && \text{(A.12)}\\ &= f_0 - \tau\left(v_x\frac{\partial f_0}{\partial E_F}\frac{\partial E_F}{\partial x} + v_x\frac{\partial f_0}{\partial T}\frac{\partial T}{\partial x} - \frac{e\mathcal{E}}{m}\frac{\partial f_0}{\partial E}\frac{\partial E}{\partial v_x}\right) \\ &= f_0 - \tau\left(v_x\frac{\partial f_0}{\partial E_F}\frac{\partial E_F}{\partial x} + v_x\frac{E-E_F}{T}\frac{\partial f_0}{\partial E}\frac{\partial T}{\partial x} - e\mathcal{E}\frac{\partial f_0}{\partial E}v_x\right) && \text{(A.13)}\\ &= f_0 - \tau v_x\left(-\frac{\partial f_0}{\partial E}\frac{\partial E_F}{\partial x} - \frac{E-E_F}{T}\frac{\partial f_0}{\partial E}\frac{\partial T}{\partial x} - e\mathcal{E}\frac{\partial f_0}{\partial E}\right) \\ &= f_0 - \tau v_x\frac{\partial f_0}{\partial E}\left(\frac{\partial E_F}{\partial x} + \frac{E-E_F}{T}\frac{\partial T}{\partial x} + e\mathcal{E}\right) \\ &= f_0 - \tau v_x\frac{\partial f_0}{\partial E}\left(-e\frac{\partial \Phi}{\partial x} + \frac{E-E_F}{T}\frac{\partial T}{\partial x}\right) \end{aligned}$$

where the following relations have been used: $\vec{F} = -e\mathcal{E}$, $\partial E/\partial v_x = mv_x$, $\partial f_0/\partial E_F = -\partial f_0/\partial E$ (a mathematical consequence of f_0 being the Fermi distribution) and $-\partial\Phi/\partial x = \frac{1}{e}\partial E_F/\partial x + \mathcal{E}$ (Φ is the electrochemical potential). Also, in this case only electrons are

considered, though the derivation is equally valid for holes after making the appropriate sign change for q.

The total electrical current in the x-direction can be written as an integral over energy and solid angle of the individual carrier flux defined in equation (A.9), where each electron carries a charge of $-e$:

$$\begin{aligned} J_e(x) &= \frac{1}{4\pi}\oint\left(\int_0^\infty qv_x g(E) f\, dE\right) d\Omega \\ &= -\frac{e}{4\pi}\oint\left(\int_0^\infty v_x g(E) f\, dE\right) d\Omega \\ &= -\frac{e}{4\pi}\int_0^{2\pi}\int_0^{\pi}\left(\int_0^\infty v_x g(E) f\, dE\right)\sin\theta d\theta d\phi \\ &= -\frac{e}{4\pi}\int_0^{2\pi}\int_0^{\pi}\left(\int_0^\infty v_x g(E)\left[f_0 - \tau v_x\frac{\partial f_0}{\partial E}\left(-e\frac{\partial\Phi}{\partial x} + \frac{E-E_F}{T}\frac{\partial T}{\partial x}\right)\right] dE\right)\sin\theta d\theta d\phi \end{aligned} \tag{A.14}$$

f_0 naturally drops out of the integration at this point because it is the equilibrium distribution, and therefore represents equal amounts of energy going in both the positive and negative direction. $v_x = v\cos\theta$ can also be used here to further write:

$$\begin{aligned} J_e(x) &= -\frac{e}{2}\int_0^{\pi}\left(\int_0^\infty v^2\cos^2\theta g(E)\tau\frac{\partial f_0}{\partial E}\left(-e\frac{\partial\Phi}{\partial x} + \frac{E-E_F}{T}\frac{\partial T}{\partial x}\right) dE\right)\sin\theta d\theta \\ &= -\frac{e}{3}\int_0^\infty v^2 g(E)\tau\frac{\partial f_0}{\partial E}\left(-e\frac{\partial\Phi}{\partial x} + \frac{E-E_F}{T}\frac{\partial T}{\partial x}\right) dE \end{aligned} \tag{A.15}$$

(note that $\int\cos^2\theta\sin\theta d\theta = -\frac{1}{3}\cos^3\theta$)

$$J_e(x) = -\left[-\frac{e^2}{3}\int_0^\infty v^2 g(E)\tau\frac{\partial f_0}{\partial E}dE\right]\frac{\partial\Phi}{\partial x} - \left[\frac{e}{3T}\int_0^\infty v^2(E-E_F) g(E)\tau\frac{\partial f_0}{\partial E}dE\right]\frac{\partial T}{\partial x} \tag{A.16}$$

Similarly, for the heat flux, each electron in the conduction band carries energy equal

to $(E - E_F)$ so the total thermal current is:

$$\begin{aligned}
J_q(x) &= \frac{1}{4\pi}\oint\left(\int_0^\infty (E-E_F)\, v_x g(E)\, f\, dE\right) d\Omega \qquad (A.17)\\
&= \frac{1}{4\pi}\int_0^{2pi}\int_0^{p} i\left[\int_0^\infty (E-E_F)\, v_x g(E)\, f dE\right]\sin\theta d\theta d\phi\\
&= \frac{1}{2}\int_0^{\pi}\left[\int_0^\infty (E-E_F)\, v_x g(E)\, f dE\right]\sin\theta d\theta\\
&= \frac{1}{2}\int_0^{\pi}\left[\int_0^\infty (E-E_F)\, v_x^2 g(E)\,\tau\frac{\partial f_0}{\partial E}\left(-e\frac{\partial\Phi}{\partial x}+\frac{E-E_F}{T}\frac{\partial T}{\partial x}\right) dE\right]\sin\theta d\theta\\
&= \frac{1}{2}\int_0^{\pi}\left[\int_0^\infty (E-E_F)\, v^2\cos^2\theta g(E)\,\tau\frac{\partial f_0}{\partial E}\left(-e\frac{\partial\Phi}{\partial x}+\frac{E-E_F}{T}\frac{\partial T}{\partial x}\right) dE\right]\sin\theta d\theta\\
&= \frac{1}{3}\int_0^{\infty} (E-E_F)\, v^2 g(E)\,\tau\frac{\partial f_0}{\partial E}\left(-e\frac{\partial\Phi}{\partial x}+\frac{E-E_F}{T}\frac{\partial T}{\partial x}\right) dE\\
&= -\left[\frac{e}{3}\int_0^{\infty} (E-E_F)\, v^2 g(E)\,\tau\frac{\partial f_0}{\partial E} dE\right]\frac{\partial\Phi}{\partial x}\\
&\quad -\left[-\frac{1}{3T}\int_0^{\infty} (E-E_F)^2\, v^2 g(E)\,\tau\frac{\partial f_0}{\partial E} dE\right]\frac{\partial T}{\partial x}
\end{aligned}$$

Now that both the equation for the current and heat flux have been derived, it is possible to determine the expressions for the macroscopic transport coefficients. Setting the current J_q to 0 in equation (A.17) and taking the ratio of the electric field and the temperature gradient gives us the expression for the Seebeck coefficient, defined as α:

$$\alpha = -\frac{\frac{\partial\Phi}{\partial x}}{\frac{\partial T}{\partial x}} = -\frac{1}{eT}\frac{\int_0^\infty (E-E_F)\, v^2 g(E)\,\tau\frac{\partial f_0}{\partial E} dE}{\int_0^\infty v^2 g(E)\,\tau\frac{\partial f_0}{\partial E} dE} \qquad (A.18)$$

This expression for the Seebeck coefficient can be thought of as the average energy carried per electron divided by the electrical conductivity at each energy level, effectively making the Seebeck coefficient a measure of the average heat flux per electron.

Similarly, setting the temperature gradient equal to zero yields the definition of the electrical conductivity σ:

$$\sigma = -\frac{e^2}{3}\int_0^\infty v^2 g(E)\,\tau\frac{\partial f_0}{\partial E} dE \qquad (A.19)$$

Eliminating $\partial\Phi/\partial x$, $J_q(x)$ can be put into its most commonly encountered form in

terms of $J_e(x)$ and $\partial T/\partial x$:

$$J_q(x) = -\frac{1}{e}\frac{\int_0^\infty (E-E_F)\, v^2 g(E)\, \tau \frac{\partial f_0}{\partial E} dE}{\int_0^\infty v^2 g(E)\, \tau \frac{\partial f_0}{\partial E} dE} J_e(x) \quad \text{(A.20)}$$
$$-\frac{1}{3T}\left[\frac{\left(\int_0^\infty (E-E_F)\, v^2 g(E)\, \tau \frac{\partial f_0}{\partial E} dE\right)^2}{\int_0^\infty v^2 g(E)\, \tau \frac{\partial f_0}{\partial E} dE} - \int_0^\infty (E-E_F)^2\, v^2 g(E)\, \tau \frac{\partial f_0}{\partial E} dE\right]\frac{\partial T}{\partial x}$$

The expression in front of $J_e(x)$ is defined as the Peltier coefficient π:

$$\pi = -\frac{1}{e}\frac{\int_0^\infty (E-E_F)\, v^2 g(E)\, \tau \frac{\partial f_0}{\partial E} dE}{\int_0^\infty v^2 g(E)\, \tau \frac{\partial f_0}{\partial E} dE} \quad \text{(A.21)}$$

and the expression in front of $\partial T/\partial x$ is defined as the electron thermal conductivity k_e:

$$k_e = \frac{1}{3T}\left[\frac{\left(\int_0^\infty (E-E_F)\, v^2 g(E)\, \tau \frac{\partial f_0}{\partial E} dE\right)^2}{\int_0^\infty v^2 g(E)\, \tau \frac{\partial f_0}{\partial E} dE} - \int_0^\infty (E-E_F)^2\, v^2 g(E)\, \tau \frac{\partial f_0}{\partial E} dE\right] \quad \text{(A.22)}$$

If equation (A.22) is expanded and simplified, it can be found that all of the terms with E_F cancel and this results in the following expression for k_e:

$$k_e = \frac{1}{3T}\left[\frac{\left(\int_0^\infty E v^2 g(E)\, \tau \frac{\partial f_0}{\partial E} dE\right)^2}{\int_0^\infty v^2 g(E)\, \tau \frac{\partial f_0}{\partial E} dE} - \int_0^\infty E^2 v^2 g(E)\, \tau \frac{\partial f_0}{\partial E} dE\right] \quad \text{(A.23)}$$

A.3 Temperature Dependence of Transport Coefficients

The purpose of solving the Boltzmann equation for the transport coefficients is to derive the temperature dependence of α, σ and k. For electrons and holes, which follow Fermi-Dirac statistics, the equilibrium distribution and density of states functions are:

$$f_0 = \frac{1}{\exp\frac{E-E_F}{kT}+1} \quad \text{(A.24)}$$

$$g(E) = \frac{4\pi (2m^*)^{\frac{3}{2}} E^{\frac{1}{2}}}{h^3} \quad \text{(A.25)}$$

where m^* is the effective mass and h is Planck's constant. If the energy bands for the material are parabolic then m^* is not a function of E and can be removed from the

integral. The simplest relaxation time approximation uses a power law dependence on E:

$$\tau = \tau_0 E^r \tag{A.26}$$

where r depends on the type of scattering that is dominant.

Substituting equations (A.24) - (A.26) into equations (A.18), (A.19) and (A.23), we have:

$$\alpha = -\frac{1}{eT}\left[\frac{\int_0^\infty E^{r+5/2}\frac{\partial f_0}{\partial E}dE}{\int_0^\infty E^{r+3/2}\frac{\partial f_0}{\partial E}dE} - E_F\right] \tag{A.27}$$

$$\sigma = -\frac{2^{9/2}e^2\pi\left(m^*\right)^{1/2}\tau_0}{3h^3}\int_0^\infty E^{r+1/2}\frac{\partial f_0}{\partial E}dE \tag{A.28}$$

$$k_e = -\frac{2^{9/2}\pi\left(m^*\right)^{1/2}\tau_0}{3Th^3}\left[\frac{\left(\int_0^\infty E^{r+5/2}\frac{\partial f_0}{\partial E}dE\right)^2}{\int_0^\infty E^{r+3/2}\frac{\partial f_0}{\partial E}dE} - \int_0^\infty E^{r+7/2}\frac{\partial f_0}{\partial E}dE\right] \tag{A.29}$$

Equations (A.27) - (A.29) all contain an integral in the form of $\int_0^\infty E^n\frac{\partial f_0}{\partial E}dE$. This integral can be solved through first integrating by parts:

$$\begin{aligned}\int_0^\infty E^n\frac{\partial f_0}{\partial E}dE &= \left(nE^{n-1}f_0\right)_0^\infty - n\int_0^\infty E^{n-1}f_0dE \\ &= -n\int_0^\infty E^{n-1}f_0dE \\ &= -n\int_0^\infty \frac{E^{n-1}}{\exp\frac{E-E_F}{kT}+1}dE\end{aligned} \tag{A.30}$$

and then making the substitution $x = \frac{E}{kT}$:

$$-n\int_0^\infty \frac{E^{n-1}}{\exp\frac{E-E_F}{kT}+1}dE = -n\left(kT\right)^n\int_0^\infty \frac{x^{n-1}}{e^{x-\eta}+1}dx \tag{A.31}$$

where η is the normalized Fermi energy. The integral $\int_0^\infty \frac{x^{n-1}}{e^{x-\eta}+1}dx$ can be solved with help from polylogarithms [17]:

$$\int_0^\infty \frac{x^{n-1}}{e^{x-\eta}+1}dx = -\Gamma\left(n\right)Li_n\left(-e^\eta\right) \tag{A.32}$$

so the integral in (A.30) becomes:

$$\int_0^\infty E^n \frac{\partial f_0}{\partial E} dE = -n\,(kT)^n\,\Gamma\,(n)\,Li_n\,(-e^\eta) \tag{A.33}$$

Using equation (A.33), equations (A.27) - (A.29) can be rewritten as:

$$\alpha = -\frac{k}{e}\,(kT)^{1/2}\left[\frac{\left(r+\frac{5}{2}\right)\Gamma\left(r+\frac{5}{2}\right)Li_{r+\frac{5}{2}}\,(-e^\eta)}{\left(r+\frac{3}{2}\right)\Gamma\left(r+\frac{3}{2}\right)Li_{r+\frac{3}{2}}\,(-e^\eta)} - \eta\right] \tag{A.34}$$

$$\sigma = -\frac{2^{9/2}e^2\pi\,(m^*)^{1/2}\,\tau_0}{3h^3}\,(kT)^{r+1/2}\left(r+\frac{1}{2}\right)\Gamma\left(r+\frac{1}{2}\right)Li_{r+\frac{1}{2}}\,(-e^\eta) \tag{A.35}$$

$$k_e = -\frac{2^{9/2}\pi\,(m^*)^{1/2}\,\tau_0}{3Th^3}\,(kT)^{r+7/2}\left[\frac{\left(\left(r+\frac{5}{2}\right)\Gamma\left(r+\frac{5}{2}\right)Li_{r+\frac{5}{2}}\,(-e^\eta)\right)^2}{\left(r+\frac{3}{2}\right)\Gamma\left(r+\frac{3}{2}\right)Li_{r+\frac{3}{2}}\,(-e^\eta)} - \left(r+\frac{7}{2}\right)\Gamma\left(r+\frac{7}{2}\right)Li_{r+\frac{7}{2}}\,(-e^\eta)\right] \tag{A.36}$$

Thus, assuming the scattering parameter r is known, these relationships contain the temperature dependence of the transport coefficients.

A.4 Two-Band Effects

So far the transport coefficients have only been derived with the electron being the only carrier. The contributions made by holes (or any other type of charged carrier) to the thermoelectric effect can be added to the transport equations by considering the partial transport coefficients. For electrons in the conduction band, we have:

$$J_e = \sigma_e\left(-\frac{\partial\Phi}{\partial x}\right) - \sigma_e\alpha_e\frac{\partial T}{\partial x} \tag{A.37}$$

$$q_e = \alpha_e T J_e - k_e\frac{\partial T}{\partial x} \tag{A.38}$$

where the relation $\pi = \alpha T$ comes from equations (A.18) and (A.21), and α_e, σ_e and k_e refer to the expressions in (A.18), (A.19) and (A.23), respectively, or the electronic contribution to each of the transport coefficients. For holes in the valence band, the equations are identical:

$$J_h = \sigma_h \left(-\frac{\partial \Phi}{\partial x} \right) - \sigma_h \alpha_h \frac{\partial T}{\partial x} \tag{A.39}$$

$$q_h = \alpha_h T J_h - k_h \frac{\partial T}{\partial x} \tag{A.40}$$

In the absence of a temperature gradient, the total current is:

$$J = J_e + J_h = (\sigma_e + \sigma_h) \left(-\frac{\partial \Phi}{\partial x} \right) \tag{A.41}$$

so the total conductivity is:

$$\sigma = (\sigma_e + \sigma_h) \tag{A.42}$$

In the absence of current, which requires the hole and electron currents to be equal and opposite,

$$(\sigma_e + \sigma_h) \left(-\frac{\partial \Phi}{\partial x} \right) = (\sigma_e \alpha_e + \sigma_h \alpha_h) \frac{\partial T}{\partial x} \tag{A.43}$$

The Seebeck coefficient is defined as:

$$\alpha = -\frac{\frac{\partial \Phi}{\partial x}}{\frac{\partial T}{\partial x}} = \frac{\sigma_e \alpha_e + \sigma_h \alpha_h}{\sigma_e + \sigma_h} \tag{A.44}$$

which is the average of the two partial Seebeck coefficient, weighted by their individual conductivities. Next, in order to arrive at an effective electron thermal conductivity, again the current must be zero, so that the electron and hole currents are equal and opposite:

$$J_e = -J_h = \frac{\sigma_e \sigma_h}{\sigma_e + \sigma_h} (\alpha_h - \alpha_e) \frac{\partial T}{\partial x} \tag{A.45}$$

Substituting this back into the expression for the electron heat flux, we find:

$$q = q_e + q_h = -\left[k_e + k_h + \frac{\sigma_e \sigma_h}{\sigma_e + \sigma_h} (\alpha_h - \alpha_e)^2 \right] \frac{\partial T}{\partial x} \tag{A.46}$$

Therefore the combined thermal conductivity is:

$$k = -\left[k_e + k_h + \frac{\sigma_e \sigma_h}{\sigma_e + \sigma_h} \left(\alpha_h - \alpha_e\right)^2\right] \tag{A.47}$$

A.5 Phonon Thermal Conductivity

Electrons are not the only carriers of heat in a lattice. Phonons, or lattice vibrations are the other carrier of heat in semiconductors. Phonons, which obey Bose-Einstein statistics, have the distribution function in equation (A.48):

$$f_0 = f_0\left(\omega, T\right) = \frac{1}{\exp\frac{\hbar\omega}{kT} + 1} \tag{A.48}$$

Using the same procedure as the was used for the charge carriers, f can be written under a temperature gradient as:

$$f = f_0 - \tau\left(v_x \frac{\partial f_0}{\partial T}\frac{\partial T}{\partial x}\right) = f_0 + \tau v_x \frac{\omega}{T}\frac{\partial f_0}{\partial \omega}\frac{\partial T}{\partial x} \tag{A.49}$$

and the heat flux is:

$$J_q\left(x\right) = \frac{1}{4\pi}\oint\left(\int_0^{\omega_{max}} \hbar\omega v_x g\left(\omega\right) f d\omega\right) d\Omega \tag{A.50}$$

where ω_{max} is the maximum phonon frequency, which varies depending on the approximation used. One example is the Debye frequency, the upper bound for phonon frequencies in the Debye model. Using the same procedure as in equation (A.17), we can write:

$$J_q\left(x\right) = \frac{\hbar}{3T}\left[\int_0^{\omega_{max}} \omega^2 v^2 g\left(\omega\right)\tau\frac{\partial f_0}{\partial \omega} d\omega\right]\frac{\partial T}{\partial x} \tag{A.51}$$

Equation (A.51) is effectively Fourier's law:

$$q = -k_p \frac{\partial T}{\partial x} \tag{A.52}$$

where

$$k_p = -\frac{\hbar}{3T}\left[\int_0^{\omega_{max}} \omega^2 v^2 g\left(\omega\right)\tau\frac{\partial f_0}{\partial \omega} d\omega\right] \tag{A.53}$$

This reverts back to the simple form for the lattice thermal conductivity from the kinetic model if v and τ can be pulled out of the integral:

$$k_p = \frac{1}{3}\tau v^2 C_v = \frac{1}{3} C_v v \Lambda \tag{A.54}$$

where Λ is the mean free path length τv and C_v is the lattice specific heat. The total thermal conductivity in a semiconductor is a sum of the lattice and electron thermal conductivities:

$$k = k_e + k_p \tag{A.55}$$

A.6 Full Transport Equations

For completeness the full transport equations in three dimensions will be restated here, using the symbol **E** for the electric field.

$$\mathbf{J} = \sigma \mathbf{E} - \sigma \alpha \nabla T \tag{A.56}$$

$$\mathbf{q} = \alpha T \mathbf{J} - k \nabla T \tag{A.57}$$

where **J** and **q** are the electrical current density and heat flux density, respectively, **E** is the electric field, T is temperature, and σ,α and k are the electrical conductivity, Seebeck coefficient and thermal conductivity.

Appendix B

Brief Discussion of the Kelvin Relation

Thomson's original proof of the Kelvin relation, that the Peltier coefficient of a metal is equal to its Seebeck coefficient multiplied by the temperature, was based on thermodynamic reasoning. However, Thomson included assumptions not covered by thermodynamics and he considered the relation a conjecture to be proven or disproven by experiment, although subsequent experiments have shown the Kelvin relation to be true.

We now know that the Thomson relation is just one example of a class of relations known as the Onsager reciprocal relations [18], which are central to the thermodynamics of irreversible processes. We summarize Onsager's theorem here as follows:

Suppose a system has a set of generalized currents, J_1,J_2,J_n flowing within it which are influenced by a set of generalized forces, X_1,X_2,X_n, resulting in a linear system of equations:

$$J_i = \sum_j L_{ij} X_i \tag{B.1}$$

And furthermore suppose that J_i and X_i have been defined in such a way that the

rate of entropy generation in the system is:

$$\delta S = \sum_i L_i X_i \tag{B.2}$$

Then the matrix of coefficients L_{ij} is symmetrical.

In the context of thermoelectricity, there are two currents, heat and electrical current. For electrical current, the change in entropy is:

$$\delta S = \frac{\mathbf{J} \cdot \mathbf{E}}{T} \tag{B.3}$$

and for heat the change in entropy is:

$$\delta S = \mathbf{q} \nabla \frac{1}{T} \tag{B.4}$$

Therefore the four forces and currents for the thermoelectric system are:

$$J_1 = \mathbf{J} \tag{B.5}$$

$$J_2 = \mathbf{q} \tag{B.6}$$

$$X_1 = \frac{\mathbf{E}}{T} \tag{B.7}$$

$$X_2 = \nabla \frac{1}{T} = -\frac{\nabla T}{T^2} \tag{B.8}$$

Written in terms of the macroscopic transport coefficients (α, σ, π, k), the equations are:

$$J_1 = \sigma T X_1 + \sigma \alpha T^2 X_2 \tag{B.9}$$

$$J_2 = \sigma \pi T X_1 + k T^2 X_2 \tag{B.10}$$

and the Onsager reciprocal relation for the system is:

$$\sigma \alpha T^2 = \sigma \pi T \tag{B.11}$$

or

$$\alpha T = \pi \tag{B.12}$$

Appendix C

Efficiency and Figure of Merit

C.1 Thermoelectric

With a few assumptions, a first-order approximation of efficiency can be made for a single thermocouple acting as a generator. Here we present the procedure most commonly found in textbooks on the subject. The most common configuration is an n-type semiconductor and a p-type semiconductor as the two arms of the thermocouple with a high side temperature T_H and low side temperature T_L, as in Figure 2. The thermocouple is then connected across a load R_L so that useful work can be produced. In this case, the definition of the efficiency is:

$$\eta = \frac{\text{Power absorbed by load}}{\text{Power supplied by hot junction}} \tag{C.1}$$

Starting from equation (1.1):

$$\mathbf{J} = \sigma\mathbf{E} - \sigma\alpha\nabla T \tag{C.2}$$

If the current $\mathbf{J}$ is set to zero (i.e. there is an open circuit) then equation (C.2) can be rewritten in both the p and n-type legs as:

$$\mathbf{E} = \alpha\nabla T \tag{C.3}$$

Performing the same integral as in equation (1.8), we find that the voltage across the resistor provided by the generator as a result of the Seebeck effect is:

$$V = \int_{T_L}^{T_H} (\alpha_p - \alpha_n)\, dT = (\alpha_p - \alpha_n)\,(T_H - T_L) \tag{C.4}$$

If the series resistance of the two branches is R then the current that flows is:

$$I = \frac{(\alpha_p - \alpha_n)\,(T_H - T_L)}{R + R_L} \tag{C.5}$$

and so the power delivered to the load is:

$$P = I^2 R_L = \left(\frac{(\alpha_p - \alpha_n)\,(T_H - T_L)}{R + R_L}\right)^2 R_L \tag{C.6}$$

Next, the heat delivered by the source must be considered. Besides the conducted heat, there is also the heat created by the Peltier effect and the Joule heat. This can be written as:

$$q = K\,(T_H - T_L) + (\alpha_p - \alpha_n)\,T_H I - \frac{1}{2} I^2 R \tag{C.7}$$

where K is the thermal conductance of the p and n branches in parallel:

$$K = \frac{k_p A_p}{l_p} + \frac{k_n A_n}{l_n} \tag{C.8}$$

The expression for the efficiency is then:

$$\eta = \frac{\left(\frac{(\alpha_p - \alpha_n)(T_H - T_L)}{R + R_L}\right)^2 R_L}{K\,(T_H - T_L) + (\alpha_p - \alpha_n)\,T_H \frac{(\alpha_p - \alpha_n)(T_H - T_L)}{R + R_L} - \frac{1}{2}\left(\frac{(\alpha_p - \alpha_n)(T_H - T_L)}{R + R_L}\right)^2 R} \tag{C.9}$$

The efficiency depends on the way the load is matched to the internal resistance of the thermocouple. If the ratio R_L/R is called m, then $d\eta/dm = 0$ may be solved [19] to find:

$$(R_L/R)_{optimal} = \sqrt{1 + \frac{Z\,(T_L + T_H)}{2}} \tag{C.10}$$

where Z is known as the figure of merit, given by:

$$Z = \frac{\alpha_{pn}^2}{RK} \tag{C.11}$$

Substituting the above back into the expression for efficiency and making the appropriate algebraic manipulations, we have:

$$\eta = \frac{T_H - T_L}{T_H} \frac{\sqrt{1 + \frac{Z(T_L+T_H)}{2}} + 1}{\sqrt{1 + \frac{Z(T_L+T_H)}{2}} + \frac{T_L}{T_H}} \tag{C.12}$$

This final expression is notable because it is in the form of something multiplied by the Carnot efficiency. Equally important, it can be seen that if the cold plate and hot plate temperatures are kept constant, increasing Z is the only way to increase maximum efficiency. Finally, it's important to note that the figure of merit defined above is for a pair of materials and using this definition is cumbersome when trying to identify good individual thermoelectric materials. For this reason the figure of merit for a single material is defined as:

$$Z = \frac{\alpha^2 \sigma}{k} \tag{C.13}$$

C.2 Rankine Cycle

Here we briefly discuss the calculation of efficiency for the Rankine Cycle. The derivation here is for completeness only and is essentially identical to the treatment given in [20].

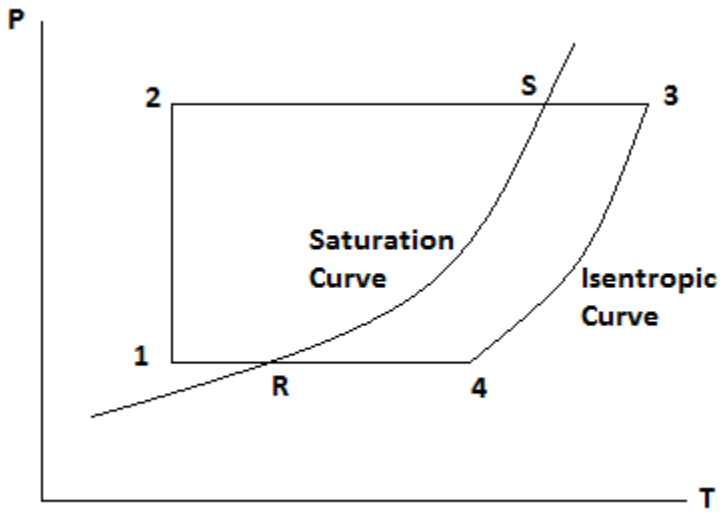

Figure C.1: Rankine Cycle in PT Coordinates

Figure C.1 shows the Rankine Cycle in a P-T diagrams. Leg 1-2 represents pumping, 2-3 reheating, vaporization and superheating, 3-4 isentropic expansion and 4-1 cooling and condensation. There are phase changes during the cooling and reheating stages at points R and S. In terms of the enthalpy, the efficiency is:

$$\eta = \frac{(H_3 - H_4) - (-\Delta W_p)}{H_3 - H_2} \tag{C.14}$$

where $(-\Delta W_p)$ denotes parasitic losses including pumping and circulation losses. Depending on the working fluid used, equation (C.14) alone can be used to approximate the efficiency by consulting steam tables. However, with some assumptions equation (C.14) can be expanded. Since enthalpy is a state function whose changes are independent of path, $H_3 - H_2$ can be written as:

$$H_3 - H_2 = (H_3 - H_4) + (H_4 - H_R) + \lambda_R + (H'_R - H_1) - (H_2 - H_1) \tag{C.15}$$

where λ_R denotes the latent heat of vaporization and H_R and H'_R denote the enthalpy of the saturated vapour and liquid at equilibrium during condensation (leg 4-1). By

definition, $H_R = H'_R + \lambda_R$. Another way to express the heat input at pressure P_2 is:

$$\begin{aligned} H_3 - H_2 &= (H_3 - H_S) + \lambda_S + (H'_S - H_2) \\ &= (C_p)_V|_{P_2}(T_3 - T_S) + \lambda_S + (C_p)_L|_{P_2}(T_S - T_2) \end{aligned} \tag{C.16}$$

where $(C_p)_V|_{P_2}$ represents the mean heat capacity of the vapour phase, $(C_p)_L|_{P_2}$ represents the mean heat capacity of the liquid phase and $\lambda_S \approx \lambda_R$.

Equating the two expressions for $H_3 - H_2$ in equations (C.15) and (C.16) and solving for $H_2 - H_1$, we find:

$$\begin{aligned} H_2 - H_1 &= (H_3 - H_4) + (H_4 - H_R) + \lambda_R + (H'_R - H_1) \\ &\quad - [(H_3 - H_S) + \lambda_S + (H'_S - H_2)] \\ &= C_p(T_3 - T_4) + (H_4 - H_R) + \lambda_R + (H'_R - H_1) \\ &\quad - \left[(C_p)_V|_{P_2}(T_3 - T_S) + \lambda_S + (C_p)_L|_{P_2}(T_S - T_2)\right] \end{aligned} \tag{C.17}$$

If it can be assumed that $(C_p)_V|_{P_2} \approx C_p$ and $T_1 = T_2 = T_4 = T_R$ then equation (C.17) can be further simplified to:

$$H_2 - H_1 \approx \left[C_p - (C_p)_L|_{P_2}\right](T_S - T_4) + (\lambda_R - \lambda_S) \tag{C.18}$$

The expressions for $(H_2 - H_1)$ in equations (C.17) and (C.18) represent the energy required for the pumping phase (leg 1-2) and will be labeled $-\Delta W_{pump}$. Some further assumptions can now be made to simplify the expression for the efficiency. If there is no cooling of the exhaust vapours and no supercooling of the condensate, then the simplifications $H_4 - H_R = 0$ and $H'_R - H_1$ can be made, and equation (C.14) can be rewritten:

$$\eta = \frac{(H_3 - H_4) - (-\Delta W_p)}{(H_3 - H_4) + \lambda_R - (-\Delta W_{pump})} \tag{C.19}$$

Furthermore, if parasitic losses can be neglected and assuming ideal isentropic expansion, the expression simplifies to:

$$\eta = \frac{C_p(T_3 - T_4)}{C_p(T_3 - T_4) + \lambda_R - (-\Delta W_{pump})} \tag{C.20}$$

Appendix D

Finite Element Model of Thermoelectric Generator

COMSOL, a multiphysics finite element simulation suite, was used to perform the finite element simulations for the thermoelectric module. COMSOL doesn't include an application mode specific to thermoelectricity, so the general PDE mode must be used instead. COMSOL also doesn't allow arbitrary equations to be entered but rather provides a general equation for which the coefficients can be set. For steady state analysis, the subdomain equation provided by the PDE mode is:

$$\nabla \left(-c\nabla \mathbf{u} - \alpha \mathbf{u} + \gamma\right) + a\mathbf{u} + \beta \cdot \nabla \mathbf{u} = f \tag{D.1}$$

where $\mathbf{u}$ is the dependant variable. The idea is to rewrite the PDE for any system in this form and then provide COMSOL with the coefficients c, α, a, β and source term f. Since everything must necessarily be in terms of the gradient of the dependant variables, the coupled equations of heat and current flow have to be written in terms of the scalar variables T and V.

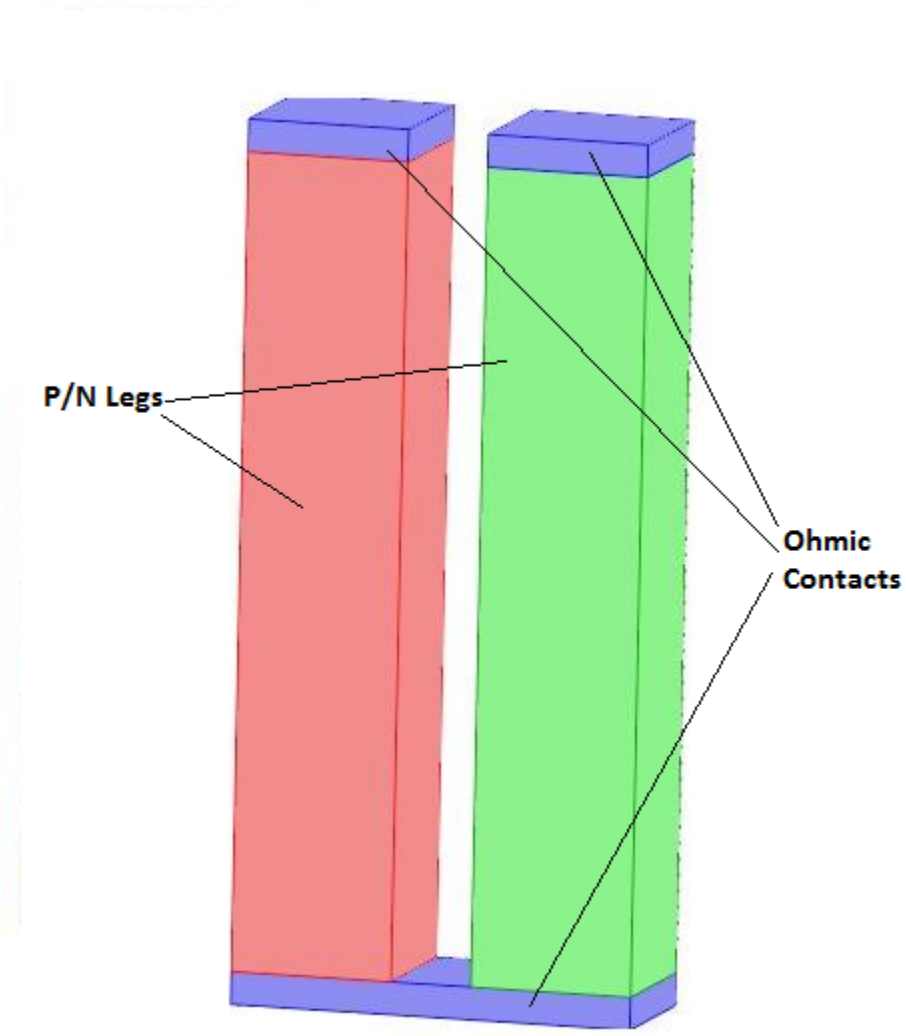

Figure D.1: FEM Geometry

D.1 Subdomain Equations

Revisiting equations (1.1) and (1.2):

$$\mathbf{J} = \sigma\mathbf{E} - \sigma\alpha\nabla T \tag{D.2}$$

$$\mathbf{q} = \alpha T\mathbf{E} - \kappa\nabla T. \tag{D.3}$$

There are also the constitutive relations from Maxwell's equations and from the definition of heat flow:

$$\nabla \cdot \mathbf{J} = 0 \tag{D.4}$$

$$\nabla \cdot \mathbf{q} = \dot{Q} = \mathbf{E} \cdot \mathbf{J} \tag{D.5}$$

Finally, the definition of the electric field in terms of the electric potential:

$$\mathbf{E} = -\nabla V \tag{D.6}$$

Substituting equations (D.2) and (D.3) into (D.4) and (D.6) and making the necessary manipulations, we arrive at the coupled equations:

$$\nabla \cdot \left(\left(\sigma\alpha^2 T + k\right)\nabla T\right) = \sigma\left(\nabla V \cdot \nabla V + \alpha \nabla V \cdot \nabla T\right) \tag{D.7}$$

$$\nabla \cdot (\sigma\alpha\nabla T) + \nabla \cdot (\sigma \nabla V) = 0 \tag{D.8}$$

For three dimensions this can be written out as:

$$\nabla\cdot\left(\left(\sigma\alpha^2 T + k\right)\nabla T\right) = \sigma\left(\left(\frac{\partial V}{\partial x}\right)^2 + \left(\frac{\partial V}{\partial y}\right)^2 + \left(\frac{\partial V}{\partial z}\right)^2 + \alpha\left(\frac{\partial T}{\partial x}\frac{\partial V}{\partial x} + \frac{\partial T}{\partial y}\frac{\partial V}{\partial y} + \frac{\partial T}{\partial z}\frac{\partial V}{\partial z}\right)\right) \tag{D.9}$$

$$\nabla \cdot (\sigma\alpha\nabla T) + \nabla \cdot (\sigma \nabla V) = 0 \tag{D.10}$$

We assume that the transport coefficients (α, σ, k) are dependent on only temperature and not position so they can be taken outside of the gradients. Now that the coupled equations are in this form, it is easy to see what the coefficients would be in COMSOL's PDE. First of all, since there are two dependent variables, T and V, $\mathbf{u}$ becomes a matrix instead of a scalar:

$$\mathbf{u} = \begin{bmatrix} T \\ V \end{bmatrix} \tag{D.11}$$

and the coefficients are:

$$c = \begin{bmatrix} \sigma\alpha^2 T + k & \sigma\alpha T \\ \sigma\alpha & \sigma \end{bmatrix} \tag{D.12}$$

$$c = \begin{bmatrix} \sigma\left(\left(\frac{\partial V}{\partial x}\right)^2 + \left(\frac{\partial V}{\partial y}\right)^2 + \left(\frac{\partial V}{\partial z}\right)^2 + \alpha\left(\frac{\partial T}{\partial x}\frac{\partial V}{\partial x} + \frac{\partial T}{\partial y}\frac{\partial V}{\partial y} + \frac{\partial T}{\partial z}\frac{\partial V}{\partial z}\right)\right) \\ 0 \end{bmatrix} \tag{D.13}$$

while the other coefficients are equal to 0. Writing out $\nabla(-c\nabla\mathbf{u}) = f$ then reconstructs the coupled equations.

D.2 Boundary Conditions

COMSOL provides support for the two most common types of boundary conditions, Dirichlet and Neumann.

Dirichlet Boundary Condition:

$$\mathbf{n} \cdot (-c\nabla\mathbf{u} - \alpha\mathbf{u} + \gamma) + q\mathbf{u} = \mathbf{g} - h^T\mathbf{u} \tag{D.14}$$

$$h\mathbf{u} = \mathbf{r} \tag{D.15}$$

Neumann Boundary Condition:

$$\mathbf{n} \cdot (-c\nabla\mathbf{u} - \alpha\mathbf{u} + \gamma) + q\mathbf{u} = \mathbf{g} - h^T\mathbf{u} \tag{D.16}$$

The coefficient matrices c, α and γ have already been set in the subdomain equations, q isn't necessary, and h doesn't need to be anything but the identity matrix, so the two types of boundary conditions are simplified to:

$$\begin{bmatrix} T \\ V \end{bmatrix} = \begin{bmatrix} r_1 \\ r_2 \end{bmatrix} \tag{D.17}$$

$$\begin{bmatrix} \mathbf{n} \cdot \mathbf{q} \\ \mathbf{n} \cdot \mathbf{J} \end{bmatrix} = \begin{bmatrix} g_1 \\ g_2 \end{bmatrix} \tag{D.18}$$

allowing the potentials or fluxes on a boundary to be set directly with the correct units, which is convenient. The thermal and electrical insulation boundary condition which is used along insulated surfaces would be:

$$\begin{bmatrix} \mathbf{n} \cdot \mathbf{q} \\ \mathbf{n} \cdot \mathbf{J} \end{bmatrix} = \begin{bmatrix} 0 \\ 0 \end{bmatrix} \tag{D.19}$$

Appendix E

Experimental Setup

The purpose of performing experiments was to ascertain experimental values for the transport coefficients and to obtain results to compare to the finite-volume model. The tests carried out with our experimental apparatus include measurements of the Seebeck coefficient and conductivity of the thermoelectric module as a function of temperature and measurements in time of the open-circuit voltage while heating from room temperature for comparison to the model.

In the experimental setup, two power resistors connected electrically in parallel are used to supply a constant heat flux to the hot side of the thermoelectric module. On the cold side, a heat sink and fan are used to remove heat. A hollow oven brick is placed over the heating elements and polyurethane foam insulation is placed beside the thermoelectric module to provide thermal insulation. It is assumed that the insulation is sufficient enough that nearly all of the electrical power put into the resistors (V^2/R) is delivered to the thermoelectric module as heat.

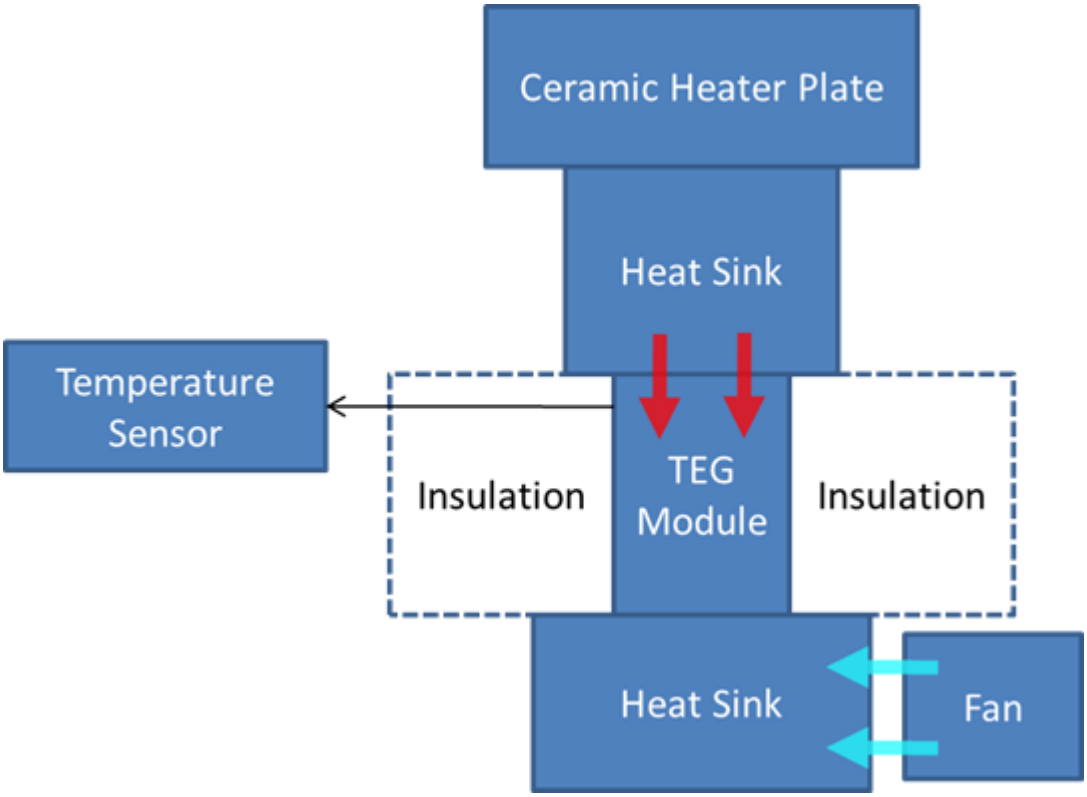

Figure E.1: Experimental Block Diagram

A potentiometer connected to the terminals of the thermoelectric module allows the operating point to be varied. From this setup it is possible to perform tests to generate heat flux-voltage-current curves as well as measure the Seebeck coefficient and thermal and electrical conductivities.

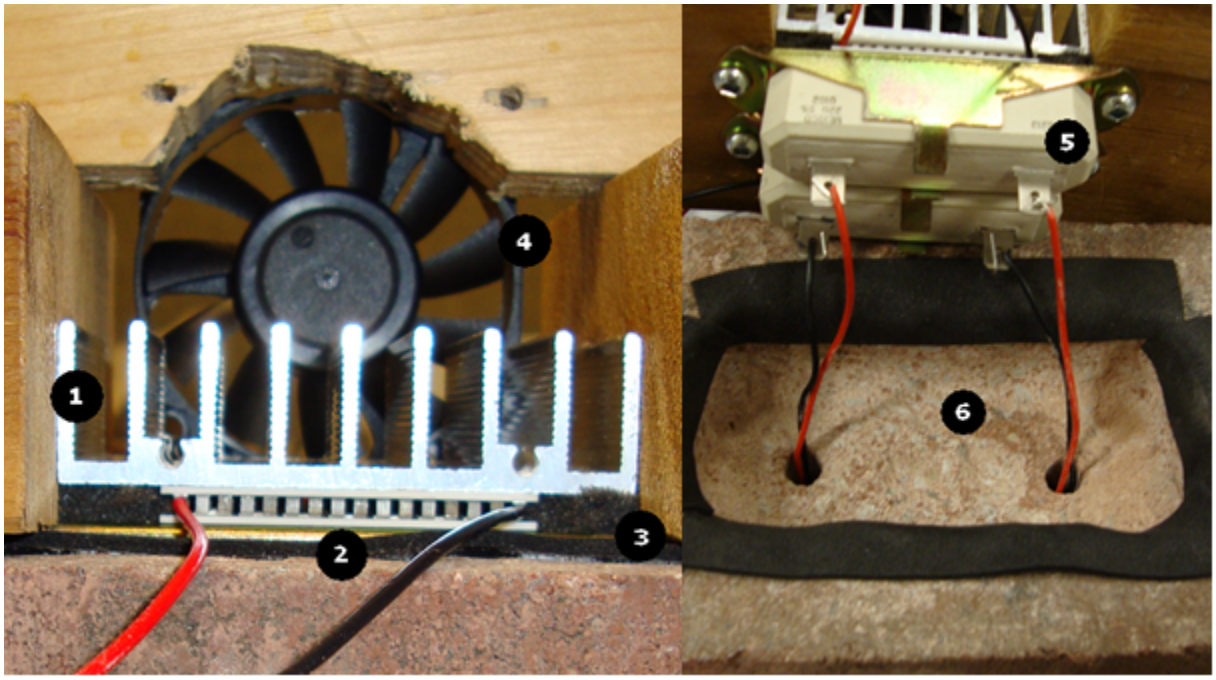

Figure E.2: Experimental Setup

1. Heat sink
2. Thermoelectric module
3. Foam insulation
4. Cooling fan
5. Resistive heating element
6. Oven brick

In order to approximate the heat capacitance values of the components in the experimental apparatus, they were individually weighed and multiplied by their specific heat capacities. The measured values are given in the following table. A small, estimated value was used for the TE module because a value for C_p could not be obtained for it.

Component	Material	Mass (g)	$C_p(kJ/(kgK)$	Capacitance (J/K)
Resistors	Steatite Ceramic	72.0 (x2)	0.9[21]	130
Heat Sink	Aluminum	36.5	0.9	33
TE Module	Bi_2Te_3 & Ceramic	19.0		20

Appendix F

Matlab Code

F.1 thermoelectric1.m

thermoelectric1.m is the main function which contains the equations derived in Chapter 2. It outputs dx_dt which is the difference vector for the state variable x. dx_dt is passed to MATLAB's ODE solver. Some of the internal variables are also declared in this function.

```
function [dx_dt]=thermoelectric1(t,x,Num_Elements, Q_in, T_amb, I, Re_tot,
 Rth_tot, N_high, N_low, R_high_tot, R_low_tot)
N=Num_Elements;
dx_dt=zeros(2*N+N_high+N_low+2,1);
alpha=zeros(N,1);
Re = Re_tot/N;
Rth = Rth_tot/N;



R_high=R_high_tot/N_high;
R_low=R_low_tot/N_low;
C_high=180/N_high;    %high side heat capacity
```

```
C_low=40/N_low;     %low side heat capacity
Cth=20/N;     %thermal circuit heat capacity
Ce=500e-5*N;    %electrical circuit capacitance


for i=1:N      %Sets up alpha as a function of T.
   alpha(i)=Sfun(x(N_high+i));
   %alpha(i)=0.022;
end

%Sets up the placeholder variables for T at boundary B and T at boundary C
 (instead of writing out this whole expression inside each of the other
 expressions)
%This is with the linear equation for T_1-1/2, this expression and the
 derivation are in the thesis document
Tb = (Rth*x(N_high) + R_high*x(N_high+1) + alpha(1)^2*Rth*R_high*
x(N_high+1)^2/Re - Rth*R_high*alpha(1)*x(N_high+1)*x(N_high+2*
N+N_low+1)/(2*Re))/(Rth + R_high + Rth*R_high*alpha(1)^2*x(N_high+1)/Re);
Tc = (Rth*x(N_high+N+1) + R_low*x(N_high+N) + alpha(N)^2*Rth*R_low*
x(N_high+N)^2/Re + alpha(N)*Rth*R_low*x(N_high+N)*x(N_high+2*N+N_low+2)
/(2*Re))/(Rth + R_low + alpha(N)^2*Rth*R_low*x(N_high+N)/Re);

dx_dt(1) = (Q_in + (x(2)-x(1))/R_high)/C_high;

for i=2:N_high-1
    dx_dt(i) = (x(i+1)-2*x(i)+x(i-1))/R_high/C_high;
end

dx_dt(N_high) = ((Tb-x(N_high))/(R_high/2) - (x(N_high)-x(N_high-1))/R_high)/C_high;
```

```
dx_dt(N_high+1) = (  (1/Re)*( x(N_high+N+N_low+1)^2 -alpha(1)*x(N_high+N+N_low+1)*
((x(N_high+2)+x(N_high+1))/2-Tb)/(1) ) -alpha(1)*((x(N_high+2)+x(N_high+1))/2
*(x(N_high+N+N_low+2)+x(N_high+N+N_low+1))/2 - Tb*x(2*N+N_high+N_low+1))/Re
+(alpha(1)^2/Re)*((x(N_high+2)+x(N_high+1))*(x(N_high+2)-x(N_high+1))/2-Tb*2*
(x(N_high+1)-Tb)) + (x(N_high+2)-x(N_high+1))/Rth + (Tb-x(N_high+1))/(Rth/2))/Cth;
dx_dt(N_high+N+N_low+1) = (I - x(N_high+N+N_low+1)/Re + alpha(1)*((x(N_high+2)+
x(N_high+1))/2-Tb)/Re)/Ce;

for i=N_high+2:N_high+N-1
    dx_dt(i) = ((1/Re)*( x(N+N_low+i)^2 - (1/2)*alpha(i-N_high)*x(N+N_low+i)*
(x(i+1) - x(i-1)) ) -alpha(i-N_high)*((x(i+1)+x(i))/2*(x(N+N_low+i+1)+x(N+N_low+i))/2
-(x(i)+x(i-1))/2*(x(N+N_low+i)+x(N+N_low+i-1))/2)/Re +(alpha(i-N_high)^2/Re)*
((x(i+1)+x(i)) * (x(i+1)-x(i))/2-(x(i)+x(i-1))*(x(i)-x(i-1))/2)+ (x(i+1)-2*x(i)+x(i-1))
/Rth)/Cth;
    dx_dt(i+N+N_low) = (I - x(i+N+N_low)/Re + alpha(i-N_high)*(x(i+1)-x(i-1))/(2*Re))/Ce;
end

dx_dt(N_high+2*N+N_low) = (I - x(N_high+2*N+N_low)/Re + alpha(N)*(Tc-(x(N_high+N)+
x(N_high+N-1))/2)/Re)/Ce;
dx_dt(N_high+N) = ((1/Re)*( x(N_high+2*N+N_low)^2 -alpha(N)*x(N_high+2*N+N_low)*(Tc-
(x(N_high+N)+x(N_high+N-1))/2) ) - alpha(N)*(Tc*x(2*N+N_high+N_low+2)-(x(N_high+N-1)
+x(N_high+N))/2*(x(N_high+2*N+N_low)+x(N_high+2*N+N_low-1))/2)/Re+(alpha(N)^2/Re)*
(Tc*2*(Tc-x(N_high+N))-(x(N_high+N)+x(N_high+N-1))*(x(N_high+N)-x(N_high+N-1))/2)
+ (x(N_high+N-1)-x(N_high+N))/Rth + (Tc-x(N_high+N))/(Rth/2))/Cth;
dx_dt(N_high+N+1) = (-(x(N_high+N+1) - Tc)/(R_low/2) + (x(N_high+N+2) - x(N_high+N+1))
/R_low)/C_low;

for i=N_high+N+2:N_high+N+N_low-1
    dx_dt(i) = ((x(i+1) - 2*x(i)+x(i-1))/(R_low))/C_low;
```

```
end


dx_dt(N_high+N+N_low) = ((x(N_high+N+N_low-1)
 - x(N_high+N+N_low))/(R_low) + (T_amb - x(N_high+N+N_low))
/(R_low/2))/C_low;


dx_dt(2*N+N_high+N_low+1)=(I-2*x(2*N+N_high+N_low+1)/Re+2*alpha(1)*(x(N_high+1)-Tb)/Re)
/(Ce);
dx_dt(2*N+N_high+N_low+2)=(I-2*x(2*N+N_high+N_low+2)/Re+2*alpha(1)*(Tc-x(N_high+N))/Re)
/(Ce);
```

F.2 main.m

main.m is the script that calls MATLAB's ODE solver, ode23() to solve the function defined in thermoelectric1.m. Also in this code, some variables needed for the ODE solver are declared and the material-related constants and initial conditions used in thermoelectric1.m are defined.

```
clear
clc
Simulation_Time=3000;
Num_Elements=10;
N_high=10;
N_low=10;


Q_in=20;   %input heat flux in the thermal subcircuit
I=0.00;   %current in the electrical subcircuit
Re_tot=4.4;   %Total electrical resistance
```

```
Rth_tot=2;   %Total thermal resistance
T_amb=293.15;   %ambient temperature in the thermal subcircuit
R_high_tot=0.1;   %high side thermal resistance
R_low_tot=0.8;    %low side thermal resistance

Initial_Cond=zeros(2*Num_Elements+N_high+N_low+2,1);

%set up initial conditions for temperature
%for i=N_high+Num_Elements+N_low:-1:N_high+Num_Elements+1
%    Initial_Cond(i)=T_amb+Q_in*R_low_tot/(2*N_low)+(N_high+Num_Elements+N_low-i)
*Q_in*R_low_tot/N_low;
%end
%for i=N_high+Num_Elements:-1:N_high+1
%    Initial_Cond(i)=Initial_Cond(N_high+Num_Elements+1)+Q_in*(Rth_tot/(2*Num_Elements)
+R_low_tot/(2*N_low))+(N_high+Num_Elements-i)*Q_in*Rth_tot/Num_Elements;
%end
%for i=N_high:-1:1
%    Initial_Cond(i)=Initial_Cond(N_high+1)+Q_in*(Rth_tot/(2*Num_Elements)+
R_high_tot/(2*N_high))+(N_high-i)*Q_in*R_high_tot/N_high;
%end

%set up initial conditions for voltage
%for i=N_high+Num_Elements+N_low+1:N_high+Num_Elements+N_low+Num_Elements
%    Initial_Cond(i)=I*Re_tot/Num_Elements;
%end

%Set up initial conditions for voltage boundary elements
%Initial_Cond(2*Num_Elements+N_high+N_low+1)=I*Re_tot/Num_Elements;
%Initial_Cond(2*Num_Elements+N_high+N_low+2)=I*Re_tot/Num_Elements;
```

```
%----------------------INITIAL CONDITIONS FOR TEST RUN-------------------------
-------
%set up initial conditions for temperature
for i=N_high+Num_Elements+N_low:-1:1
    Initial_Cond(i)=T_amb;
end


%set up initial conditions for voltage
for i=N_high+Num_Elements+N_low+1:N_high+Num_Elements+N_low+Num_Elements
    Initial_Cond(i)=0;
end

%Set up initial conditions for voltage boundary elements
Initial_Cond(2*Num_Elements+N_high+N_low+1)=0;
Initial_Cond(2*Num_Elements+N_high+N_low+2)=0;
%------------------------------------------------------------------------------
-------

options=odeset('MaxStep', 1);

%, 'OutputFcn',@odeplot,'OutputSel', [1 2 3 4 5 6 7]

[tg,xg]=ode23(@thermoelectric1,[0 Simulation_Time],Initial_Cond,options,Num_Elements,
 Q_in, T_amb, I, Re_tot, Rth_tot, N_high, N_low, R_high_tot, R_low_tot);

x=xg.';
V=-sum(x(N_high+Num_Elements+N_low+1:N_high+Num_Elements+N_low+Num_Elements,size(x,2)));
```

```
Vg=zeros(size(x,2),1);
for i=1:size(x,2)
    Vg(i)=-sum(x(N_high+Num_Elements+N_low+1:N_high+Num_Elements+N_low+Num_Elements,i));
end
```

F.3 Sfun.m

Sfun.m is called by thermoelectric1.m and is the function alpha(T). The function is a third order Lagrange polynomial approximation based on experimental measurements on the commercial Peltier cooler in Appendix E.

```
% This is the function alpha(T)
function [S] = Sfun(T)

if T<307.15
    T = 307.15;
elseif T > 344.65
    T = 344.65;
end

S = (-73*T^3/6e10 + 129*T^2/2e8 - 47*T/15e5 + 21/5000)/0.82;
```

Bibliography

[1] A. W. Crook (ed). *Profiting From Low-Grade Waste Heat*. London: Institute of Electrical Engineers, 1994.

[2] D. M. Rowe (ed). *CRC Handbook of Thermoelectrics*. Danvers, MA: CRC Press, 1995.

[3] R.C. O'Briena et al. "Safe radioisotope thermoelectric generators and heat sources for space applications". In: (2009).

[4] J. M. Ziman. *Thermoelectrics: Basic Principles and New Material Developments*. Oxford: Oxford Clarendon Press, 1960.

[5] Gang Chen. *Nanoscale Energy Transport and Conversion*. Oxford: Oxford University Press, 2005.

[6] Nowak W, A. Borsukiewicz, and A. A. Stachel. "Using the low-temperature Clausius-Rankine cycle to cool technical equipment". In: (2008).

[7] J. A. Chavez et al. "SPICE Model of Thermoelectric Elements Including Thermal Effects". In: (2000).

[8] Simon Lineykin and Sam Ben-Yaakov. "Analysis of Thermoelectric Coolers by a SPICE-Compatible Equivalent Circuit Model". In: (2005).

[9] D.D.L. Wijngaards et al. "Modelling of integrated Peltier elements". In: *2000 International Conference on Modeling and Simulation of Microsystems*.

[10] M. Chen et al. "Transient Behavior Study of Thermoelectric Generators through an Electro-thermal Model Using Spice". In: *25th International Conference on Thermoelectrics*.

[11] D. Mitrani et al. "One-dimensional modeling of TE devices considering temperature-dependent parameters using SPICE". In: (2009).

[12] Anthony F. Mills. *Heat and Mass Transfer*. Concord, MA: Richard D Irwin, 1995.

[13] G. S. Nolas, J. Sharp, and H. J. Goldsmid. *Electrons and Phonons; the Theory of Transport Phenomena in Solids*. Berlin: Springer, 2001.

[14] H. J. Goldsmid. *Introduction to Thermoelectricity*. Berlin: Springer, 2010.

[15] R. Mansfield and W. Williams. "The Electrical Properties of Bismuth Telluride". In: (1958).

[16] H. J. Goldsmid. "The Thermal Conductivity of Bismuth Telluride". In: *Report of the Meeting on Semiconductors*. 1957, pp. 127–131.

[17] Marc D. Ulrich, William F. Seng, and Peter A. Barnes. "One-dimensional modeling of TE devices considering temperature-dependent parameters using SPICE". In: *Journal of Computational Electronics* 1.3 (2002), pp. 431–434.

[18] L Onsager. "Reciprocal relations in irreversible processes". In: (1931).

[19] A. F. Ioffe. *Semiconductor thermoelements, and thermoelectric cooling*. 1957.

[20] E.J. Hoffman. *Power Cycles and Energy Efficiency*. San Diego: Academic Press, 1996.

[21] Werner Martienssen and Hans Warlimont. *Springer Handbook of Condensed Matter and Materials Data, Volume 1*. Berlin: Springer, 2005.